Harmful Algae 68 (2017) 152–167

Contents lists available at ScienceDirect

Harmful Algae

journal homepage: www.elsevier.com/locate/hal

Research Paper

Identification of *Azadinium* species and a new azaspiracid from *Azadinium poporum* in Puget Sound, Washington State, USA

Joo-Hwan Kim[a], Urban Tillmann[b], Nicolaus G. Adams[c], Bernd Krock[b], Whitney L. Stutts[d], Jonathan R. Deeds[d], Myung-Soo Han[a,*], Vera L. Trainer[c,*]

[a] Department of Life Science, College of Natural Sciences, Hanyang University, Seoul 04763, South Korea
[b] Alfred Wegener Institute, Helmholtz Center for Polar and Marine Research, Am Handelshafen 12, D-27570 Bremerhaven, Germany
[c] Northwest Fisheries Science Center, National Marine Fisheries Service, National Oceanic and Atmospheric Administration, 2725 Montlake Blvd. E., Seattle, WA 98112, USA
[d] United States Food and Drug Administration, Center for Food Safety and Applied Nutrition, 5001 Campus Drive, College Park, MD 20740, USA

ARTICLE INFO

Article history:
Received 25 April 2017
Received in revised form 7 August 2017
Accepted 7 August 2017
Available online 18 September 2017

Keywords:
Azadinium
Azaspiracid
Puget sound
Washington state
Harmful algae

ABSTRACT

The identification of a new suite of toxins, called azaspiracids (AZA), as the cause of human illnesses after the consumption of shellfish from the Irish west coast in 1995, resulted in interest in understanding the global distribution of these toxins and of species of the small dinoflagellate genus *Azadinium*, known to produce them. Clonal isolates of four species of *Azadinium, A. poporum, A. cuneatum, A. obesum* and *A. dalianense* were obtained from incubated sediment samples collected from Puget Sound, Washington State in 2016. These *Azadinium* species were identified using morphological characteristics confirmed by molecular phylogeny. Whereas AZA could not be detected in any strains of *A. obesum, A. cuneatum* and *A. dalianense*, all four strains of *A. poporum* produced a new azaspiracid toxin, based on LC–MS analysis, named AZA-59. The presence of AZA-59 was confirmed at low levels *in situ* using a solid phase resin deployed at several stations along the coastlines of Puget Sound. Using a combination of molecular methods for species detection and solid phase resin deployment to target shellfish monitoring of toxin at high-risk sites, the risk of azaspiracid shellfish poisoning can be minimized.

1. Introduction

In November 1995, a shellfish poisoning event of unknown etiology occurred after several people consumed cultivated mussels (*Mytilus edulis*) from the Irish west coast (McMahon and Silke, 1996). Their symptoms were similar to diarrhetic shellfish poisoning (DSP) and included nausea, vomiting, severe diarrhea and stomach cramps. Diarrhetic shellfish toxins (DSTs; okadaic acid and dinophysistoxin-2) were present at concentrations below the regulatory limit, and thus were less likely to have caused the severe intoxications. Soon after this poisoning event, the first member of a novel group of marine biotoxins, designated as azaspiracids (AZAs), was isolated and characterized from shellfish and named AZA-1 (Satake et al., 1998).

It took over a decade to positively identify a small dinoflagellate (<20 μm) *Azadinium spinosum* from the North Sea on the Scottish East Coast as a source organism for AZA (Tillmann et al., 2009). Since that time, 12 new species within the genus *Azadinium* have been isolated and characterized (Tillmann and Akselman, 2016; Luo et al., 2017). As the study of *Azadinium* intensifies, several species of this genus have been recorded in many countries including Europe (Tillmann et al., 2009, 2012b, 2014a; Percopo et al., 2013), East Asia (Potvin et al., 2012; Gu et al., 2013; Luo et al., 2013), New Zealand (Smith et al., 2015) and Central and South America (Luo et al., 2016; Tillmann et al., 2016, 2017b). Likewise, there are several reports of contamination with AZAs in shellfish from Ireland (Salas et al., 2011), the east coast of England and the west coast of Norway (James et al., 2002), Portugal (Vale et al., 2008), Morocco (Taleb et al., 2006), Canada (M. Quilliam, pers. comm.), Chile (López-Rivera et al., 2010), Japan (Ueoka et al., 2009; reported in a sponge) and China (Yao et al., 2010). Therefore, the distribution of *Azadinium* is a topic of great interest.

To date, the only *Azadinium* species known to produce AZA are *A. spinosum*, *A. poporum* and *A. dexteroporum,* and one species of the closely related genus *Amphidoma*, *Am. languida*, has also been shown to produce AZA (Krock et al., 2012; Tillmann et al., 2017a, 2012a). For many of the species one or few strains have been

* Corresponding authors.
E-mail addresses: hanms@hanyang.ac.kr (M.-S. Han), vera.l.trainer@noaa.gov (V.L. Trainer).

https://doi.org/10.1016/j.hal.2017.08.004
1568-9883/

obtained and tested, and thus it is not totally clear if and to what extent toxin production is a stable species-specific trait. For *A. poporum* and *Am. languida*, different strains of the same species may show different toxin profiles (Krock et al., 2014; Tillmann et al., 2017a). Moreover, a few non-toxigenic strains have been described for *A. poporum* (Krock et al., 2014), and a subarctic strain of *A. dexteroporum* lack AZA (Tillmann et al., 2015), whereas the Mediterranean type culture of the species produce a number of different AZA (Rossi et al., 2017).

Azaspiracid-1 is known to be toxic to human cell lines such as B lymphocyte, embryonic kidney, lung ephithelial, monocyte (Twiner et al., 2005), breast cancer (Ronzitti et al., 2007), hepatoblastoma, bladder carcinoma (Flanagan et al., 2001), neuroblastoma (Vilariño et al., 2006) and T lymphocyte (Twiner et al., 2008). AZA-2 has been shown to have very similar toxic activity as AZA-1 in terms of cytotoxicity and cytoskeleton alterations (Vilariño et al., 2008). There are few studies about the toxicity of other AZA analogues (Kilcoyne et al., 2014, 2015; Krock et al., 2015) and all of them had cytotoxic effect on Jurkat T lymphocyte cells being either higher or lower in cytotoxicity compared to AZA-1.

In the USA, diarrhetic shellfish poisoning was first confirmed in June 2011 in 3 people who ate contaminated mussels collected from a public dock in Sequim Bay, Washington (Lloyd et al., 2013; Trainer et al., 2013). Since that time, the Washington State Department of Health has reported over 100 closures of commercial and recreational shellfish harvesting sites annually resulting from shellfish contamination by diarrhetic shellfish toxins (DTX), mostly DTX-1. Anecdotal reports from consumers having DSP-like symptoms after eating Puget Sound shellfish from sites with no DTX or *Vibrio* have caused managers to suspect that additional toxins, such as AZAs, were the cause. Therefore, this study attempted to determine whether *Azadinium* species were present in Puget Sound as a first step to estimating the risk for azaspiracid shellfish poisoning in the region.

In the present study, *Azadinium* spp. were isolated from sediment samples collected in Puget Sound, Washington State. Several *Azadinium* species were positively identified, and their morphology was examined using light and electron microscopy. A new azaspiracid toxin was identified from local *A. poporum* strains and its presence was confirmed at low levels *in situ* using a solid phase resin deployed at several sites along the coastlines of Puget Sound.

2. Materials and methods

2.1. Sediment sampling

Sediment samples were collected from 15 stations in Puget Sound (Fig. 1) in January and February 2016 using a hydraulically dampened Craib corer (Craib, 1965) with a diameter of 6.2 cm or, for some of the stations, using a Van Veen grab. In the case of Dabob Bay, Quilcene Bay and Sequim Bay, samples were obtained at several stations in each bay considering the hydrographical characteristics (e.g., inner/middle/outer stations, edge/central stations). Sediment from the upper 0–1 cm of the core or grab samples was stored in the dark at 4 °C until analysis.

2.2. Detection of Azadinium in sediment samples

2.2.1. DNA extraction from sediment

One gram of sediment was transferred to 15 mL conical tubes and diluted in 10 mL of seawater that had been passed through a 25 mm filter (Whatman GF/F; nominal pore size 0.7 μm). DNA debris remaining in sediment particles was removed to prevent overestimation the result using quantitative real-time polymerase chain reaction (qPCR) analysis. To remove DNA debris, a heating and dilution method was applied (Kim et al., 2015). Briefly, 2 mL of sediment suspension were transferred to 2 mL microfuge tubes and then centrifuged (2,000*g* for 7 min). The pellets were resuspended with 1 mL double distilled water to dilute salts. The suspensions were incubated at 75 °C in a water bath for 10 min and mixed 2–3 × during incubation by inverting tubes. Samples were centrifuged (2,000*g* for 7 min) and supernatants were removed by pipetting. Sediment pellets were mixed with beads and lysis buffer from the PowerSoil® DNA Isolation Kit (MoBio,

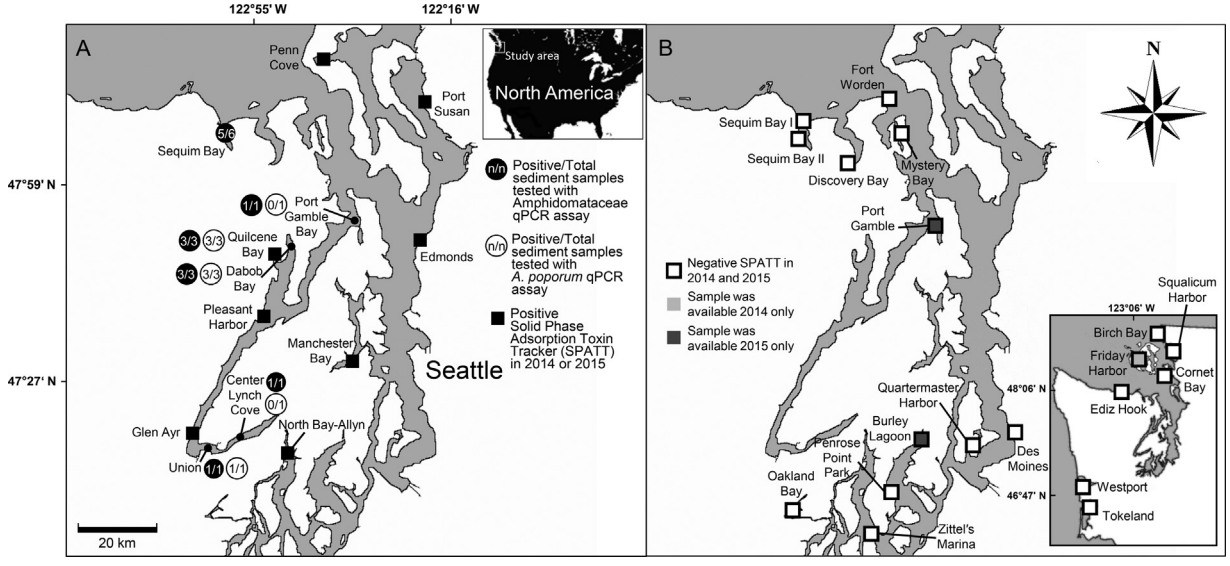

Fig. 1. Sediment sampling stations (2016) for qPCR assay and locations of Solid Phase Adsorption Toxin Tracking (SPATT) sampler deployment (2014–2015). (A) Locations where sediment samples were collected (black circles) and where AZA-59 was detected in SPATT resin (black squares) in 2014 or 2015. Numbers in circles show numbers of positive stations and total stations tested in qPCR assay using probes for Amphidomataceae (black) and *Azadinium poporum* (white). Inset shows the study area. (B) Locations where AZA-59 was not detected in SPATT in both 2014 and 2015 (white squares) with three exception stations (grey and dark grey squares). Inset shows all locations in northern Puget Sound, the Strait of Juan de Fuca and the Washington outer coast.

Carlsbad, USA) followed by DNA extraction according to the manufacturer's instructions.

2.2.2. Quantitative PCR

The presence of Amphidomataceae cells, including *Azadinium* spp. and *Amphidoma* spp., in sediment samples was determined using a SYBR green-based qPCR assay described by Smith et al. (2015). The relative abundance of *A. spinosum*, *A. obesum* and *A. poporum* was estimated using a qPCR assay based on species-specific Taq-man probes (Toebe et al., 2013).

2.3. Cell isolation from sediment and culture

Vegetative cells of *Azadinium* were obtained through the incubation of sediments presumably by cyst germination (Gu et al., 2013; Tillmann et al., 2016). Sediment suspensions (300–1000 μL) were well mixed, transferred to 6-well culture plates, and diluted in 5 mL of seawater culture medium, ESNW(-Si) enriched without silicate (Harrison et al., 1980). The well plates were incubated at 18 °C at 150–180 $\mu E\, m^{-2}\, s^{-1}$ under 12:12-h light:dark conditions. After 5–7 days, well plates were inspected using an inverted microscope (Axiovert 135, ZEISS, Germany). Cells with *Azadinium*-like motility (e.g., swimming at low speed, interrupted by short, high-speed 'jumps' in various directions) were isolated, washed and individually transferred into wells of a 96-well plate containing 200 μL of ESNW(-Si) medium using a capillary pipet. The isolated cells were incubated under the same conditions as described above.

Larger volumes of *Azadinium* strains for DNA and AZA analysis were obtained by transferring cells from 96-well plates to 6-well plates containing 5 mL of ESNW(-Si) per well, then to 50 mL culture flasks (Corning, New York, USA) containing 20 mL of the same medium under the same conditions.

For DNA extraction, 2 mL of cultures were transferred to 2 mL microtubes, centrifuged (14,000*g* for 5 min) and supernatants were decanted. DNA was extracted from the cell pellets using the methods below.

For toxin analysis, 400 mL cultures were grown under the same conditions as described above. For each harvest, cell density was determined by settling Lugol's fixed samples and counting >800 cells under an inverted microscope. Densely grown strains were harvested by centrifugation (Eppendorf 5810R, Hamburg, Germany) at 3,220*g* for 10 min and cell pellets were stored at −20 °C until analysis. For a number of strains, this procedure was repeated several times to increase the sensitivity of AZA detection by obtaining a higher biomass. The corresponding total amount of cells for harvested for each strain is listed in Suppl. Table S1.

2.4. Microscopy

Observation of living or fixed (formaldehyde or neutralized Lugol's preservative, 1% final concentration) cells from culture was carried out using a stereomicroscope (Olympus SZH-ILLD, Olympus, Hamburg, Germany) with dark field illumination, an inverted microscope (Axiovert 200 M, Zeiss, Germany) and a compound microscope (Axiovert 2, Zeiss, Germany), the latter two equipped with differential interference contrast optics.

Observation and documentation of living cells at high magnification (1,000 ×) was performed using a Zeiss Axioskop 2 (Zeiss, Göttingen, Germany). Videos were recorded using a digital camera (Gryphax, Jenoptik, Germany) at full-HD resolution. Single frame micrographs were extracted using Corel Video Studio software (Version X8). Photographs of formalin-fixed cells (1% final concentration) were taken with a digital camera (Axiocam MRc5, Zeiss, Germany).

For size measurements, exponential phase cultures were fixed by formaldehyde (1% final concentration). Cell length and width were measured at 400 × magnification using an inverted microscope (Axiovert 135, ZEISS, Germany) equipped with a digital camera (Moticam 2300, Motic Inc, Hong Kong) with imaging software (Motic Images Plus 2.0, Motic China Group Co., Ltd., Hong Kong).

For scanning electron microscopy (SEM), 15 mL of culture was collected by centrifugation at 3,220*g* for 10 min (Eppendorf 5810R, Hamburg, Germany). The supernatant was removed and the cell pellet resuspended in 60% ethanol in a 2 mL microtube for 1 h at 4 °C. Subsequently, cells were pelleted by centrifugation (16,000*g* for 5 min) and resuspended in a 60:40 mixture of deionized water and seawater for 30 min at 4 °C. After centrifugation and removal of the diluted seawater supernatant, cells were fixed with formaldehyde (2% final concentration in a 60:40 mixture of deionized water and seawater) and stored at 4 °C for 3 h. Cells were then collected on polycarbonate filters (Millipore, 25 mm diameter, 3 μm pore-size) in a filter funnel where all subsequent washing and dehydration steps were carried out. A total of eight wash steps (2 mL MilliQ-deionized water each) were followed by a dehydration series in ethanol (30, 50, 70, 80, 95, 100%; 10 min each). Filters were dehydrated with hexamethyldisilazane (HMDS), first in 1:1 HMDS:EtOH followed by two times 100% HMDS, and then stored under gentle vacuum in a desiccator. Finally, filters were mounted on stubs, sputter coated (Emscope SC500, Ashford, UK) with gold-palladium and viewed under a SEM (FEI Quanta FEG 200, Eindhoven, Netherlands). Some SEM micrographs were presented on a black background using Adobe Photoshop 6.0 (Adobe Systems, San Jose, USA).

2.5. Molecular analysis

2.5.1. DNA extraction and sequencing

Extraction of DNA was performed on the cell pellets from the cultured isolates following the protocol supplied with the DNeasy Plant Mini Kit (Qiagen, Valencia, USA). Polymerase chain reactions were performed with 50 μL reaction mixtures containing 23 μL sterile distilled water, 10 μL 5 × Phusion HF buffer (New England Biolabs, Beverly, USA), 1 μL dNTP mixture (2.5 mM each), 2.5 μL of each primer (10 pmol), 1 μL of Phusion DNA polymerase (2.0 units/50 μL) and 10 μL of template DNA. Partial LSU rDNA sequences were amplified using primers described in Scholin et al. (1994). The ITS-5.8S-ITS2 rDNA sequences were determined using primers describe in Nézan et al. (2012). PCR cycling for partial LSU and ITS-5.8S-ITS2 rDNA was carried out in an iCycler Thermal cycler (Bio-Rad, Hercules, USA) using the following conditions: ITS-5.8S-ITS2; pre-denaturation 94 °C for 2 min, 37 cycles of 94 °C for 30 s, 52 °C for 30 s, 72 °C for 2 min, and a final extension at 72 °C for 5 min, LSU; pre-denaturation 94 °C for 3.5 min, 36 cycles of 94 °C for 50 s, 45 °C for 50 s, 72 °C for 80 s, and a final extension at 72 °C for 10 min. The PCR products were purified using a QIAquick PCR Purification Kit (Qiagen, Hilden, Germany) according to the manufacturer's instructions and sequenced (MCLAB, San Francisco, USA). Editing and contig assembly of rDNA sequence fragments were carried out using Bioedit v7.2.5 (Hall, 1999).

2.5.2. DNA sequence comparisons

Full multiple alignments of the sequences obtained (Table 1) with NCBI sequences were generated using the Clustal W1.8 (Thompson et al., 1994) and Bioedit v7.2.5 (Hall, 1999). All aligned nuclear rDNA sequences were trimmed to the same length, and the gaps were deleted.

Maximum-likelihood (ML) analyses was based on the General Time Reversible model, and the best sequence-evolutional fitting model was carried out by MEGA 7.0.14 (Kumar et al., 2016).

Table 1
Strain information (LM = light microscopy; SEM = scanning electron microscopy, LSU = large subunit rDNA, ITS = internal transcribed spacer, ND = not detected, – = not analyzed).

Species	Strain	Origin Station	Length (μm) **Mean** ± SD (Min-max)	Width (μm) **Mean** ± SD (Min-max)	l/w ratio **Mean** ± SD	N	Morphological analysis		Antapical spine[a]	Sequence data	Accession number	AZA
A. cuneatum	35C4	Dabob Bay	**13.2** ± 1.4 (10.5–16.3)	**9.8** ± 1.1 (7.0–12.4)	**1.36** ± 0.10	106	LM	SEM	No	LSU, ITS	KY404229	ND
	35A2	Dabob Bay	**14.4** ± 0.9 (12.9–17.9)	**11.1** ± 0.9 (9.4–12.8)	**1.30** ± 0.10	55	LM	SEM	No	LSU, ITS	KY404228	ND
	965F5	Dabob Bay	**14.4** ± 0.9 (12.4–18.1)	**10.9** ± 0.7 (9.0–12.8)	**1.32** ± 0.06	100	LM	SEM	No	LSU, ITS	KY404225	ND
	966G8	Dabob Bay	**14.2** ± 1.7 (10.3–18.8)	**10.6** ± 1.5 (7.2–14.3)	**1.34** ± 0.10	106	LM	–	No	LSU, ITS	KY404226	ND
	968B10	Dabob Bay	–	–	–		–	–	–	LSU, ITS	KY404227	ND
A. dalianense	121F6	Center Lynch Cove	**15.6** ± 1.5 (11.0–18.9)	**11.2** ± 1.2 (8.4–14.6)	**1.40** ± 0.11	106	LM	SEM	74% (n = 121) 54% (n = 100)	LSU, ITS	KY404223	ND
	962B8	Center Lynch Cove	**15.4** ± 1.4 (12.6–19.7)	**11.3** ± 1.3 (8.3–14.6)	**1.37** ± 0.11	106	LM	SEM	20% (n = 100) 31% (n = 100) 37% (n = 100)	LSU, ITS	KY404222	ND
	481F8	Center Lynch Cove	**15.8** ± 1.5 (12.1–19.8)	**11.0** ± 1.3 (8.5–13.9)	**1.45** ± 0.12	108	LM	SEM	72% (n = 105)	LSU, ITS	KY404220	ND
	962B3	Center Lynch Cove	**16.9** ± 1.5 (13.4–20.1)	**12.2** ± 1.2 (8.8–15.8)	**1.39** ± 0.09	82	LM	SEM	74% (n = 101) 83% (n = 100)	LSU, ITS	KY404221	ND
A. obesum	481F2	Center Lynch Cove	**15.5** ± 1.2 (11.5–19.2)	**11.2** ± 1.1 (8.7–16.5)	**1.39** ± 0.10	107	LM	SEM	No	LSU, ITS	KY404219	ND
A. poporum	967B8	Dabob Bay	**17.1** ± 1.9 (12.5–21.4)	**12.8** ± 1.6 (8.7–16.6)	**1.34** ± 0.09	107	LM	SEM	No	LSU, ITS	KY404215	AZA-59
	967G9	Dabob Bay	**16.4** ± 1.6 (12.9–21.0)	**11.6** ± 1.1 (9.0–16.2)	**1.42** ± 0.10	107	LM	SEM	No	LSU, ITS	KY404216	AZA-59
	968B7	Dabob Bay	**15.2** ± 1.6 (11.4–20.3)	**11.2** ± 1.4 (8.0–15.9)	**1.37** ± 0.11	107	LM	SEM	No	LSU, ITS	KY404217	AZA-59
	121E10	Center Lynch Cove	**15.9** ± 1.2 (11.3–18.5)	**11.0** ± 1.1 (8.5–16.6)	**1.45** ± 0.12	107	LM	SEM	No	LSU, ITS	KY404218	AZA-59

[a] Each row represents spine frequency determined on independent subcultures at different times.

Bootstrap values (branch support) were obtained from 1,000 replicates. Bootstrap values >70 are indicated at each branch node. For Bayesian analysis, the best nucleotide substitution model was searched using MrModeltest (https://github.com/nylander/MrModeltest2), and Bayesian inference was performed with the GTR + I + G model for nucleotide substitutions using MrBayes v3.2.5 (Huelsenbeck and Ronquist, 2001). The Markov Chain Monte Carlo (MCMC) process was set at two chains and 10,000,000 generations were performed. The sampling frequency was 1,000 generations. Following analysis, the standard deviation of frequencies was confirmed to be <0.01, the first 25% of all trees were deleted as burn-ins, and a consensus tree was constructed. Bayesian posterior probabilities (BI) > 0.90 are indicated at each branch node. The pairwise distances (*p*-distance) from ITS1–5.8S–ITS2 sequences of different *Azadinium* species were analyzed with MEGA 7.0.14 (Kumar et al., 2016).

2.5.3. ITS2 rRNA secondary structure modeling

The beginning and end of the ITS2 region in four *A. dalianense* strains (962B3 and 962B8 from Puget Sound [this study], IFR-ADA-01C from France (Luo et al., 2017) and AZCH02 from China (Luo et al., 2013) were identified using hidden Markov models (Keller et al., 2009). The ITS2 region consisted of approximately 210 bp. The ITS2 secondary structure was predicted by homology modeling (Wolf et al., 2005). Structures were visualized using VARNA (Darty et al., 2009). The compensatory base changes were identified using the software 4SALE (Seibel et al., 2006).

2.6. Chemical analysis of azaspiracids from Azadinium spp. cultures

2.6.1. Selected reaction monitoring (SRM) measurements

Reagents e.g. formic acid (90%, p.a.), acetic acid (p.a.) and ammonium formate (p.a.) (Merck, Darmstadt, Germany) used in the analysis were of analytical grade. The solvents, methanol and acetonitrile, were of high performance liquid chromatography (HPLC) grade (Merck, Darmstadt, Germany) and deionized water was obtained from the Milli Q (Millipore, Eschborn, Germany). Mass spectral experiments performed to survey a wide array of AZA were performed using an analytical system consisting of an AB-SCIEX-4000 Q Trap, triple quadrupole mass spectrometer equipped with a TurboSpray interface coupled to an Agilent model 1100 liquid chromatograph (LC). The LC equipment included a solvent reservoir, in-line degasser (G1379A), binary pump (G1311A), refrigerated autosampler (G1329A/G1330B), and temperature-controlled column oven (G1316A).

Cell pellets were extracted with 500 μL acetone by ultrasonication (Sonotrode, Bandelin HP2070, Berlin, Germany; 70 s; 70 cycles; 10% power). After homogenization, extracts were centrifuged (Eppendorf 5415 R) at 16,100*g* at 4 °C for 10 min. Each supernatant was transferred to a 0.45 μm pore-size spin-filter (Ultrafree, Millipore, Eschborn, Germany) and centrifuged for 30 s at 800*g*. The resulting filtrate was transferred into an LC autosampler for LC–MS/MS analysis.

Separation of AZA (5 μL sample injection volume) was performed by reverse-phase chromatography on a C8 phase. The analytical column (50 × 2 mm) was packed with 3 μm Hypersil BDS 120 Å (Phenomenex, Aschaffenburg, Germany) and maintained at 20 °C. The flow rate was 0.2 mL min^{-1}, and gradient elution was performed with two eluents, where eluent 'A' was water and 'B' was acetonitrile/water (95:5 v/v), both containing 2.0 mM ammonium formate and 50 mM formic acid. Initial conditions were 8 min column equilibration with 30% B, followed by a linear gradient to 100% B in 8 min and isocratic elution until 18 min with 100% B then returning to initial conditions until 21 min (total run time: 29 min).

Azaspiracid profiles were determined using the following parameters: curtain gas: 10 psi, CAD: medium, ion spray voltage: 5500 V, temperature: ambient, nebulizer gas: 10 psi, auxiliary gas: off, interface heater: on, declustering potential: 100 V, entrance potential: 10 V, exit potential: 30 V. SRM experiments were carried out in positive ion mode by selecting the transitions shown in Suppl. Table S2. Samples of *A. poporum* cultures were calibrated against an external two point calibration curve (10 and 100 pg μL^{-1}) standard solution of AZA-2 (Certified Reference Material, CRM, IMB-NRC, Halifax, Canada) and expressed as AZA-2 equivalents. The limit of detection was defined as signal-to-noise ratio (S/N) = 3 estimated by a one point calibration with a 1 pg μL^{-1} standard solution of AZA-2.

2.6.2. Precursor ion experiments

Precursors of the fragments *m/z* 348, *m/z* 360 and *m/z* 362 were scanned in the positive ion mode from *m/z* 400 to 950 under the following conditions: curtain gas: 10 psi, CAD: medium, ion spray voltage: 5500 V, temperature: ambient, nebulizer gas: 10 psi, auxiliary gas: off, interface heater: on, declustering potential: 100 V, entrance potential: 10 V, collision energy: 70 V, exit potential: 12 V. The limit of detection was defined as signal-to-noise ratio (S/N) = 3 estimated by a one point calibration with a 500 pg μL^{-1} standard solution of AZA-1.

2.6.3. Product ion spectra

Product ion spectra were recorded in the Enhanced Product Ion (EPI) mode in the mass range from *m/z* 150 to 950 of *m/z* 860 and *m/z* 940. Positive ionization and unit resolution mode were used. The following parameters were applied: curtain gas: 10 psi, CAD: medium, ion spray voltage: 5500 V, temperature: ambient, nebulizer gas: 10 psi, auxiliary gas: off, interface heater: on, declustering potential: 100 V, collision energy spread: 0, 10 V, collision energy: 70 V.

2.7. Passive solid-phase adsorption toxin tracking (SPATT)

2.7.1. SPATT deployment

Passive SPATT samplers were prepared using a 30 cm × 15 cm piece of 75 μm Nitex® mesh (Wildco, Yulee, USA), a 10.2 cm diameter Deluxe Luxite embroidery hoop (CreateForLess, Portland, USA) and Dianon HP-20 resin (Supelco Analytical, Bellefonte, USA) prepared in a similar manner to those described in Rundberget et al. (2009). Briefly, 3 g of the resin was placed inside of the folded Nitex® mesh and secured tightly into the embroidery hoop. Less than one week prior to deployment, the resin was activated by soaking the sampler assembly in 100% HPLC grade methanol (Thermo Fisher Scientific, Waltham, USA) for 15 min then rinsed in distilled water for 5 min. The samplers were placed into airtight zip-top bags and stored at 4 °C. Prior to deployment, a ~50 g weight and a 1.5 m length of 3.175 mm diameter nylon cord were attached to the sampler assembly.

Solid-phase adsorption toxin tracking samplers were deployed at 22 stations in July 2014, 24 stations in August 2014, 26 stations in July 2015 and 25 stations in August 2015; Fig. 1 illustrates stations where SPATT samplers were recovered and analyzed. The samplers were deployed at ~1 m depth from floating docks or buoys for a period of up to 1 week. Upon retrieval, the samplers were rinsed with fresh water and stored at 4 °C until the resin was removed from the sampler. Two samplers were not recovered in July 2015 and 8 samplers (4 in July 2015 and 4 in August 2015) contained insufficient resin for analysis. For all other samplers, the HP-20 resin was placed into a pre-weighed vial and the weight of the resin determined gravimetrically. The vials containing the resin were stored at −20 °C until extraction and analysis by LC–MS/MS.

2.7.2. SPATT resin extraction

Solid-phase adsorption toxin tracking sampler resin extractions were performed following previously described methods (Fux et al., 2009; Rundberget et al., 2009). Briefly, samples were allowed to reach room temperature, then resuspended in 10 mL LC–MS grade water and transferred to a 20 mL fritted empty SPE reservoir (Agilent Bond Elut, Agilent Technologies, Santa Clara, CA) attached to a vacuum manifold, and eluted under low vacuum to rinse. Resin samples were rinsed 2 additional times (30 mL total) to remove salts. For toxin elution, 10 mL of LC–MS grade MeOH was added to each reservoir, mixed with a glass stir rod, allowed to settle for 15 min, then eluted (not under vacuum) into a glass screw topped vial at a rate of approximately 1 drop per second until MeOH reached the top of the resin. This process was repeated with an additional 10 mL of MeOH, followed with a final elution of 5 mL MeOH taking the resin to dryness under vacuum. Sub-samples of each 25 mL combined eluate were then filtered using PTFE syringe tip membrane filters (13 mm, pore size 0.2 μm, Pall Corporation, Port Washington, NY, USA) into a glass auto-sampler vial (LC–MS certified total recovery vials with pre-slit PTFE/silicone septa, Waters Corporation, Manchester, UK) for LC–MS/MS analysis.

2.8. Selected reaction monitoring (SRM) for detection and quantitation of lipophilic toxins in SPATT samples

2.8.1. Reagents

NRC-CRM-AZA-1, AZA-2, AZA-3, DTX1, DTX2 and OA were purchased from NRC-CNRC Institute for Marine Biosciences (Halifax, NS, Canada). Optima grade solvents used for sample preparation and LC–MS/MS analysis were purchased from Fisher Scientific (Pittsburgh, USA). Ammonium formate (purity ≥ 99.0%) and formic acid (purity ca. 98%) were purchased from Sigma-Aldrich (St. Louis, USA).

2.8.2. A. poporum *cell extract*

As a positive control for the detection and confirmation of AZA-59 presence in SPATT samples, a cell pellet from 300 mL of *A. poporum* isolate 121E10 was extracted by sonicating in 2 volumes (750 μL each) of LC–MS grade MeOH on ice, using a probe sonicator (Heat Systems Cell Disruptor, Model W-225R, Ultrasonics, Inc. Plainview, USA), followed by centrifugation and filtration into an auto-sampler vial as described above.

2.8.3. Instrumental analysis

An Acquity UPLC with a 150 mm × 1 mm i.d., 1.7 μm (130 Å) BEH C18 analytical column (Waters Corporation) was used for reverse phase separation. The column was maintained at 40 °C with a flow rate of 0.12 mL min^{-1}. A gradient elution was performed with two eluents; eluent 'A' was water with 2.0 mM ammonium formate and 50 mM formic acid and 'B' was acetonitrile:water (95:5 v/v) containing 2.0 mM ammonium formate and 50 mM formic acid. Weak needle and strong needle wash solvent compositions matched that of eluent 'A' and 'B', respectively. Azaspiracids were eluted using a linear gradient from 50% B to 99% B in 10 min, followed by a 30 s hold at 99% B and re-equilibration to starting conditions for a total run time of 15 min. The auto-sampler was maintained at 10 °C, and 5 μL sample injections were made using partial loop injections.

An AB Sciex QTrap 5500 equipped with a Turbo V ionization source (Framingham, USA) was used for mass spectrometric analysis of extracts from SPATT resin and the *A. poporum* cell pellet. Turbo V ion source parameters were optimized in positive ion mode for AZAs. The curtain gas was set at 30 arbitrary units (au), ion spray voltage at 5500 V, source temperature at 300 °C, and gas 1 and 2 pressures at 60 au. SPATT resin extracts were initially screened for AZA-1, AZA-2, AZA-3 and AZA-59 by SRM experiments carried out using the transitions listed in Suppl. Table S3. The Selected reaction monitoring (SRM) parameters were as follows: 100 ms dwell time, 80 V declustering potential, 10 V entrance potential, high CAD gas (12 au), 70 V collision energy and 15 V collision cell exit potential. To determine the retention time for AZA-59 and verify that the screening method was sufficient for detection, an extracted cell pellet of *A. poporum*, described above, was analyzed using the same SRM method. For quantitation of AZA-59 in SPATT extracts, the dwell time was reduced to 50 ms to increase the number of points across each peak. AZA-59 concentrations were determined by external calibration with AZA-1 (Certified Reference Material, IMB-NRC, Halifax, Canada). A 200 ng mL^{-1} stock solution of AZA-1 was used to prepare calibration curve standards at 0.05, 0.10, 0.20, 0.39, 0.78, 1.56, 3.13, 6.25, 12.5, 25, 50 and 100 ng mL^{-1}. Analyst 1.6.2 was used for data acquisition and chromatographic peak integration. Peak areas were exported to Excel and calibration curves were fitted using least squares linear regression ($R^2 \geq 0.99$) and a 1/x weighting to ensure correct curve fit at low concentrations.

To evaluate the concentrations of AZA-59 in SPATT resin extracts relative to other lipophilic toxins, a second injection of each extract was made in order to quantitate DSTs; i.e., DTX-1, DTX-2 and OA, which preferentially ionize in negative mode. The same LC parameters were used as described above; however the gradient was adjusted to improve separation of DSTs. The column was equilibrated at 50% B for 2 min, followed by a step gradient of 50–70% B in 4 min and 70–99% B in 2 min. The column was held at 99% B for 2 min and re-equilibrated to starting conditions for a total run time of 15 min. The Turbo V ion source parameters were set as follows: curtain gas 25 au, ion spray voltage −4500 V, source temperature 550 °C, and gas 1 and 2 pressure 40 au. For SRM, a dwell time of 100 ms, declustering potential of −110 V, entrance potential of −10 V, and high CAD gas (12 au) were used. The transitions monitored for each DST and collision energy is shown in Suppl. Table S3. For quantitation of DSTs, external calibration was performed using a multi-toxin stock solution of DTX-1, DTX-2 and OA (200 ng mL^{-1} each). From this stock, calibration curve standards were prepared at 0.39, 0.78, 1.56, 3.13, 6.25, 12.5, 25, 50, 100 and 200 ng mL^{-1} for 2014 analyses. The calibration curve concentrations were lowered for quantitative analyses of the 2015 SPATT after initial analyses indicated lower concentrations of endogenous DTX-1. Standards were prepared at 0.20, 0.39, 0.78, 1.56, 3.13, 6.25, 12.5 and 25 ng mL^{-1}.

For the definition of "trace" and "detected" levels, values were given for toxin concentration when the quantitation ion was detected at or above a signal-to-noise (S/N) of 10 and the confirmatory ion was detected at or above a S/N of 3. Trace levels were reported for samples presumably containing the toxin on the basis of correct retention time and the presence of the quantitation ion at a S/N ≥ 10, but confirmatory ion S/N < 3, or both quantitation and confirmatory ions present at a S/N ≥ 3.

3. Results

3.1. qPCR screening and isolation of Azadinium *species from puget sound*

Almost all stations showed positive signal using the SYBR green qPCR assay for Amphidomataceae (Fig. 1) and Taq-man probe qPCR for *A. poporum* (Fig. 1), while *A. obesum* and *A. spinosum* were not detected in qPCR assays. Sediment samples from Dabob Bay (*A. poporum*) and Center Lynch Cove (Amphidomataceae) stations showed the highest signal (estimates based on C_t value, data not shown). The incubation experiments were conducted on sediment samples from more than 10 stations, but only sediment samples from Dabob Bay and Center Lynch Cove stations yielded *Azadinium* strains (Fig. 1). As a result, 33 clonal strains were established, 14 of

which were confirmed as *Azadinium* species, including *A. cuneatum* (5 strains), *A. dalianense* (4 strains), *A. poporum* (4 strains) and *A. obesum* (1 strain). Identification of most strains was based on morphology as examined by LM and SEM and was confirmed for all strains by rRNA sequence comparison (Table 1).

3.2. Morphological characterization

3.2.1. General morphological characteristics of Azadinium spp.

All *Azadinium* strains displayed a similar and conspicuous swimming behavior consisting of a slow movement interrupted by short "jumps" in various directions. Moreover all strains were similar in size, shape and general appearance (Fig. 2A, E, I; Fig. 3A, H, Suppl. Fig. S1). Cells of all strains were small (cell length of about 10–20 μm, Table 1) and ovoid to elliptical in shape (Figs. 2, 3, Suppl. Fig. S1). Typically, the episome was slightly larger than the hyposome, with convex sides ending in a distinctly pointed apex which was clearly visible in LM. For all strains the cingulum was deep and wide, accounting for roughly 1/5 to 1/4 of the cell length. Cells of all strains had a central or more posterior located large and round to elliptical nucleus and a presumably single chloroplast which was partially arranged, lobed and which normally extended into both the epi- and hyposome. The colour of the cells of all strains generally was yellowish-green but for some it was also deep orange in appearance (Suppl. Fig. S1). Despite all these similarities, the four species could be clearly differentiated based on some specific morphological characteristics.

3.2.2. Azadinium cuneatum

All strains of *A. cuneatum* obtained from Dabob Bay and Center Lynch Cove shared an identical morphology as observed in LM (Suppl. Fig. S1M–U). In accordance with the species description, cells consistently lacked an antapical spine. One large pyrenoid with a starch sheath (visible as a ring-like structure) was located in the episome (Fig. 2A). Because of their high similarity with *A. poporum* the morphological species designation of *A. cuneatum*

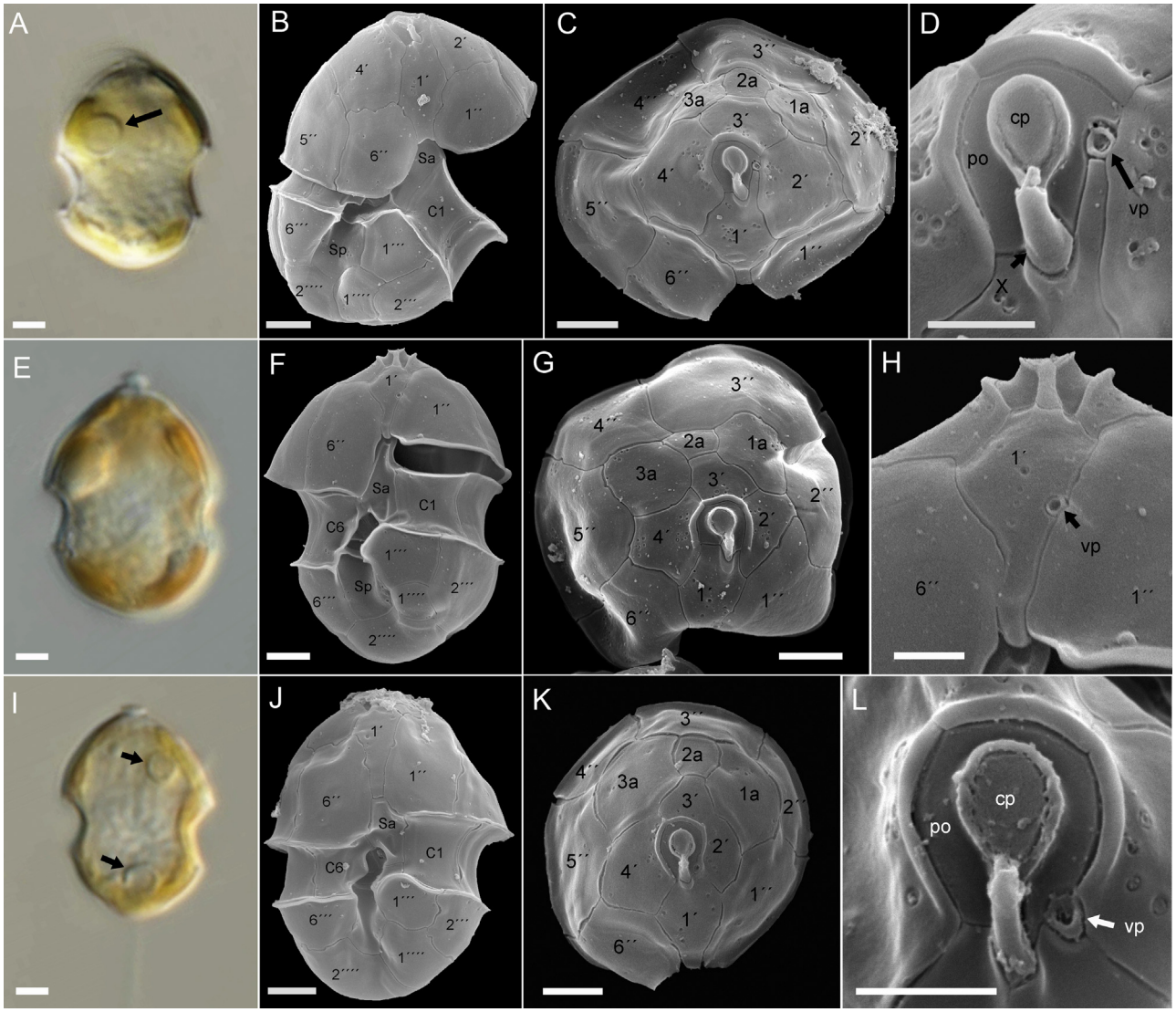

Fig. 2. Light (LM) and scanning electron micrographs (SEM) of three of the *Azadinium* species identified from Puget Sound. (A–D) *Azadinium cuneatum* (strain 965F5). (A) LM, living cell, note the pyrenoid (arrow) and (B–D) SEM of theca in (B) ventral view and (C) apical view. (D) Detailed view of the apical pore complex with the ventral pore (vp). (E–H) *Azadinium obesum* (strain 481F2). (E) LM, living cell and (F–H) SEM of theca in (F) ventral and (G) apical view. (H) Detailed ventral view of Plate 1′ with the ventral pore (vp). (I–L) *Azadinium poporum* (strain 967B8). (I) LM, living cell, note the presence of two pyrenoids (arrows) and (J–L) SEM of theca in (J) ventral view and (K) apical view. (L) Detailed view of the apical pore complex with the ventral pore (vp). Plate labels according to the Kofoidean system. cp = cover plate, X = X-plate, vp = ventral pore, po = pore plate. Scale bars = 2 μm, except D, H and L, where it is 1 μm.

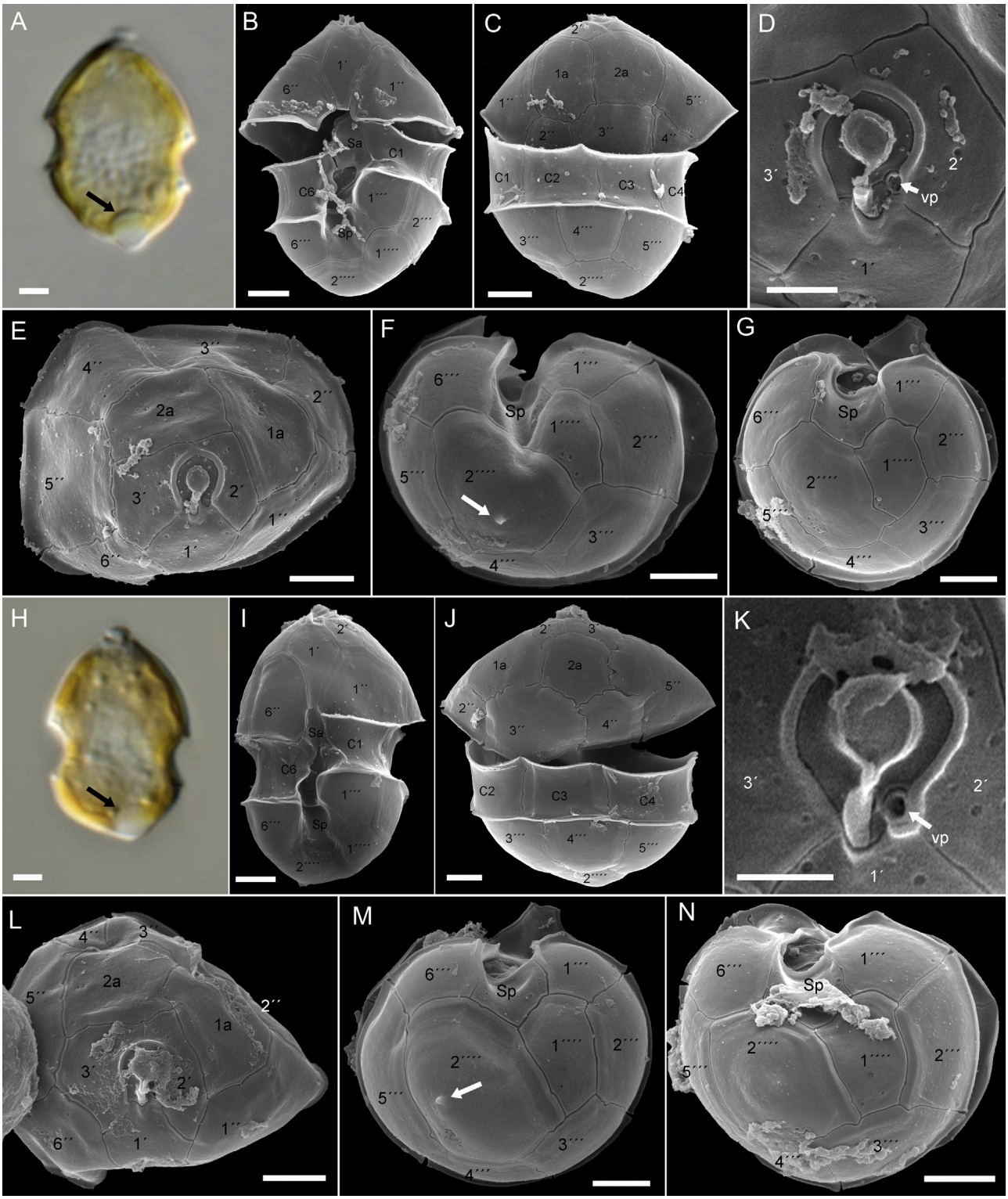

Fig. 3. Light (LM) and scanning electron micrographs (SEM) of two ribotypes of *Azadinium dalianense* from Puget Sound. (A-G) *Azadinium dalianense* strain 962B8 (ribotype A). (A) LM, living cell with pyrenoid (arrow) and (B–G) SEM of theca in (B) ventral view and (C) dorsal view. (D) Detailed apical view with the ventral pore (vp). (E) Apical view of the epithecal plates. (F) and (G) Antapical view of the hypopthecal plates. Note the spine (white arrow in F) on Plate 2′′′′, which is missing in (G). (H–L) *Azadinium dalianense* strain 962B3 (ribotype B). (H) LM, living cell with pyrenoid (arrow). (I–N) SEM of theca in (I) ventral view and (J) dorsal view. (K) Detailed apical view with the ventral pore (vp). (L) Apical view of the epithecal plates. (M) and (N) Antapical view of the hypopthecal plates. Note the spine (white arrow in M) on Plate 2′′′′, which is missing in (N). Plate labels according to the Kofoidean system. vp = ventral pore, Scale bars = 2 μm, except D and K, where it is 1 μm.

required examination by SEM, which was performed for three of the strains (Table 1). The Kofoidean plate pattern was Po, cp, X, 4′, 3a, 6′′, 6C, 5S, 6′′′, 2′′′′ (Fig. 2B, C, Suppl. Fig. S2). As the most distinctive morphological feature, *A. cuneatum* had a conspicuously formed first apical plate, which was asymmetrically elongated and tapered on its left lateral side. The ventral pore was located at

the tip of this elongated 1′ plate quite far inside the pore plate (Fig. 2D). The first and the last intercalary plates were relatively small in size, and consistently the first anterior intercalary plate (1a) was not in contact with the first precingular plate (1″) (Fig. 2C).

3.2.3. Azadinium obesum

One strain of *A. obesum* was obtained from the Center Lynch Cove station. No pyrenoid was visible in cells of this strain using light microscopy (Fig. 2E). A detailed SEM examination revealed the Kofoidean plate pattern as Po, cp, X, 4′, 3a, 6″, 6C, 5S, 6‴, 2′′′′ (Fig. 2F–H, Suppl. Fig. S3). As a distinctive morphological feature, the ventral pore was located ventrally at the margin of Plate 1′ and 1″. Plate 1′ had a narrow posterior part (Fig. 2H). Epithecal intercalary plates were relatively small and the first of them (1a) was not in contact with Plate 1″ (Fig. 2G). The small central anterior intercalary Plate 2a occurred in two arrangements, either being tetragonal and only contacting Plate 3′′ of the precingular series, or being pentagonal and in contact to two plates of the precingular series (3″ and 4″) (Fig. 2G, Suppl. Fig. S3E).

3.2.4. Azadinium poporum

Four strains of *A. poporum* were obtained from Dabob Bay and Center Lynch Cove. All *A. poporum* strains were indistinguishable with respect to all morphological details revealed through light and electron microscopy (Suppl. Figs. S1 and S8 –S11). Cells of all strains were variable in size (Suppl. Fig. S1) with strain 967B8 being slightly larger compared to the others (Table 1). There was no antapical spine, and pyrenoid(s) were always present in the cell and were located in the episome and/or the hyposome. The number of pyrenoids per cell was at least one but two pyrenoids were observed more frequently (Fig. 2I). Detailed SEM revealed the Kofoidean plate pattern as Po, cp, X, 4′, 3a, 6″, 6C, 5S, 6‴, 2′′′′(Fig. 2J-L, Suppl. Figs. S8–S11). Cells of all strains conformed to the original *A. poporum* description with respect to the position of the ventral pore, which was located at the junction of the pore plate and the first two apical plates (Fig. 2L). The larger right antapical Plate 2′′′′ typically had a distinct group of pores on the dorsal side (Suppl. Figs. S8–S11).

3.2.5. Azadinium dalianense

Four of the strains from Center Lynch Cove were identified as *A. dalianense*. They all shared the same morphological features described as distinctive for *A. dalianense* (Fig. 3, Suppl. Figs. S4–S7). The general shape of cells of all *A. dalianense* strains was characteristic as the hypocone was asymmetrically pointed with a small bulb. At the end of this bulb there occasionally was a small spine visible in LM (Suppl. Fig. S1A–L). One pyrenoid was consistently located posteriorly in the hyposome, which in living cells was sometimes difficult to see (Fig. 3A, H). Electron microscopy revealed the distinctive epithecal plate pattern of this species which consisted of only three apical plates and two large anterior intercalary plates (Fig. 3E, L, Suppl. Figs. S4–S7). Of the latter, Plate 1a was pentagonal and slightly larger than the hexagonal Plate 2a (Fig. 3C, E, J, L, Suppl. Figs. S4–S7). The ventral pore was located at the junction of the plates Po, 1′ and 2′ (Fig. 3D, K). Consistent with the species description Plate 2″ and 4″ of the precingular series were distinctly smaller compared to the other precingular plates (Fig. 3C, J). Cells of all four strains had an antapical spine located on the large antapical Plate 2′′′′. In addition there was typically a distinct group of pores located on the dorsal side of Plate 2′′′′ (Fig. 3G, M, Suppl. Figs. S4–S7). Size and development of the spine, however, was quite variable ranging from well-developed to only rudimentary (Suppl. Figs. S4–S7), and a significant proportion of cells of all strains lacked any signs of a spine (Fig. 3G, N). A quantification of the frequency of spine presence (Table 1) revealed some variability within strains but also indicated that there were strains with a relatively low (962B8) and high frequency (962B3) of spines.

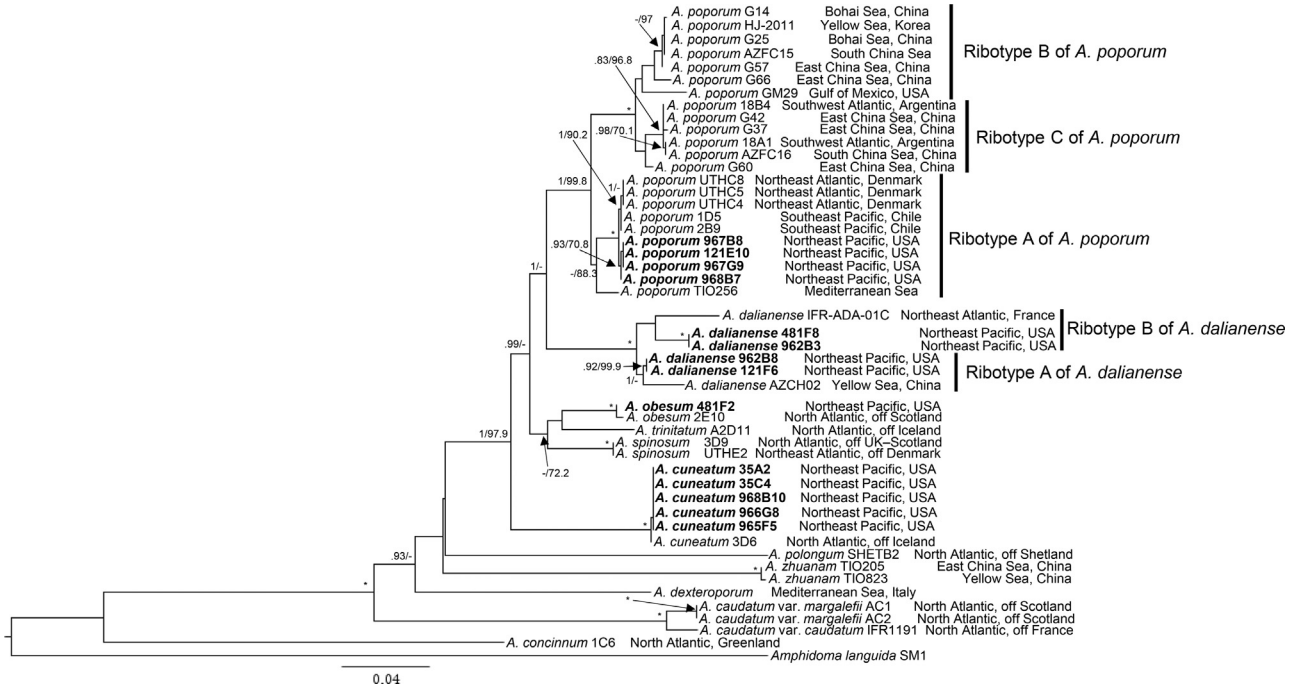

Fig. 4. The maximum likelihood (ML) phylogenetic tree based on the informative ITS and partially complete large subunit rDNA sequences (total length 1,029 bp) showing the relationships of *Azadinium* species including Northeast Pacific strains (bold). The phylogeny is rooted with *Amphidoma languida*. The best model, as chosen by MEGA 7.0.14, was GTR + G + I. Support values shown are Bayesian inference (BI)/maximum likelihood (ML) values. Only values > 70% (ML) and 0.60 (BI) are shown. Asterisks indicate maximal support (pp = 1.00 in BI and bootstrap = 100% in ML respectively).

3.3. Molecular analysis and phylogeny

The ML and BI analyses, which are based on ITS + LSU sequences, generated similar phylogenetic trees . The monophyletic nature of *A. poporum* (pp = 1.00 in BI) and other *Azadinium* species that includes new strains was confirmed (Fig. 4). The new Puget Sound strains were assigned to *A. poporum* (strain 967B8, 121E10, 967G9 and 968B7), *A. dalianense* (strain 481F8, 962B3, 962B8 and 121F6), *A. obesum* (strain 481F2) and *A. cuneatum* (strain 35A2, 35C4, 968B10, 966G8 and 965F5). The Puget Sound isolates of *A. poporum* were confirmed to be members of ribotype A that includes strains from the Northeast Atlantic, the Mediterranean Sea and Chile. The strains of *Azadinium dalianense* clustered into two well-supported clades with maximal support and each clade was here newly designated as ribotype A and B. Strain 962B8 and 121F6 were members of ribotype A together with the Chinese strain AZCH02. Strains 481F8 and 962B3 were a sister group of the French strain forming ribotype B with strong support in BI analysis but not in ML (bootstrap = 54.1% in ML and pp = 0.83 in BI).

The genetic uncorrected pairwise *p*-distance of ITS region ranged from 0.046 to 0.112 between various species (Table 2). The Puget Sound *A. poporum* strains (967B8, 967G9, 968B7 and 121E10) were identical in the ITS region although they have 1 bp difference in the partial LSU (602 bp length). The *p*-distance within Puget Sound *A. poporum* strains and *A. poporum* strains from other locations ranged from 0.014 to 0.021. The *p*-distance within *A. dalianense* was variable ranging from 0.000 to 0.062. Strain 962B3 and 481F8 were identical in the ITS region, but they had a *p*-distance value of 0.043 with strain 962B8 and 121F6, and have a *p*-distance of 0.052 with strain IFR-ADA-01C and 0.062 with strain AZCH02, respectively (Table 2). The *p*-distance based on the ITS sequence of Puget Sound *A. obesum* (481F2) and North Atlantic *A. obesum* (2E10) were zero. A 1 bp deletion occurred in the ITS region of 481F2 and a 4 bp difference in the partial LSU region (716 bp length). The ITS region of the Puget Sound *A. cuneatum* and this species from the North Atlantic were identical, however they showed 1 bp difference in the partial LSU region (602 bp length).

The ITS2 secondary structure of four *A. dalianense* strains (ribotype A: AZCH02 [China], 962B8 [Seattle], ribotype B: 962B3 [Seattle], IFR-ADA-01C [France]) was predicted (Fig. 5). The overall shape was very similar for all strains but strain IFR-ADA-01C had an additional loop structure in helix III. Also, helix IV of AZCH02 and 962B8 was 1 base pair longer than it was in 962B3 and IFR-ADA-01C, and helix I of 962B3 and 962B8 was 1 base pair shorter than the other two. There were many base changes including several hemi-compensatory base changes in helix I among the four strains. There were two compensatory base changes (CBC) between AZCH02 and 962B3 located in helices I and III and one CBC between AZCH02 and IFR-ADA-01C, and one CBC between AZCH02 and 96B8, both located in helix III. There were no CBC among 962B3, 962B8 and IFR-ADA-01C.

3.4. AZA detection in Azadinium culture

Selected reaction monitoring analysis of all strains did not result in any positive results for known AZAs (Table 1) with a limit of detection in most cases well below 0.002 fg cell^{-1} (Suppl. Table S1). In order to test for possible putative novel AZAs, precursor ion experiments with the typical AZA fragments *m/z* 348, *m/z* 360 and *m/z* 362 were performed. Precursor ion experiments were negative for all strains of *A. cuneatum*, *A. obseum* and *A. dalianense* with a limit of detection for most strains below 0.3 fg cell^{-1} (Suppl. Table S1). Out of the fourteen analyzed strains, however, all four *A. poporum* strains (967B8, 967G9, 968B7 and

Table 2
Estimated uncorrected genetic pairwise *p*-distances between species of *Azadinium*, based on ITS sequences.

	Species	Strain	1	2	3	4	5	6	7	8	9	10	11	12	13	14	15	16	17	18	19	20	21	22
1	*A. cuneatum*	3D6	–																					
2	*A. cuneatum*	965F5	0.000	–																				
3	*A. cuneatum*	966G8	0.000	0.000	–																			
4	*A. cuneatum*	968B10	0.000	0.000	0.000	–																		
5	*A. cuneatum*	35A2	0.000	0.000	0.000	0.000	–																	
6	*A. cuneatum*	35C4	0.000	0.000	0.000	0.000	0.000	–																
7	*A. dalianense*	481F8	0.112	0.112	0.112	0.112	0.112	0.112	–															
8	*A. dalianense*	962B3	0.112	0.112	0.112	0.112	0.112	0.112	0.000	–														
9	*A. dalianense*	962B8	0.100	0.100	0.100	0.100	0.100	0.100	0.043	0.043	–													
10	*A. dalianense*	121F6	0.100	0.100	0.100	0.100	0.100	0.100	0.043	0.043	0.000	–												
11	*A. dalianense*	AZCH02	0.105	0.105	0.105	0.105	0.105	0.105	0.062	0.062	0.027	0.027	–											
12	*A. dalianense*	IFR-ADA-01C	0.103	0.103	0.103	0.103	0.103	0.103	0.052	0.052	0.050	0.050	0.059	–										
13	*A. obesum*	481F2	0.064	0.064	0.064	0.064	0.064	0.064	0.087	0.087	0.073	0.073	0.077	0.078	–									
14	*A. obesum*	2E10	0.064	0.064	0.064	0.064	0.064	0.064	0.087	0.087	0.073	0.073	0.077	0.078	0.000	–								
15	*A. poporum*	18A1	0.085	0.085	0.085	0.085	0.085	0.085	0.091	0.091	0.087	0.087	0.093	0.098	0.053	0.053	–							
16	*A. poporum*	G25	0.091	0.091	0.091	0.091	0.091	0.091	0.093	0.093	0.085	0.085	0.094	0.100	0.052	0.052	0.016	–						
17	*A. poporum*	G60	0.084	0.084	0.084	0.084	0.084	0.084	0.093	0.093	0.085	0.085	0.091	0.096	0.052	0.052	0.002	0.018	–					
18	*A. poporum*	TIO256	0.082	0.082	0.082	0.082	0.082	0.082	0.087	0.087	0.080	0.080	0.089	0.093	0.046	0.046	0.027	0.027	0.028	–				
19	*A. poporum*	UTHC5	0.091	0.091	0.091	0.091	0.091	0.091	0.098	0.098	0.087	0.087	0.096	0.101	0.062	0.062	0.036	0.039	0.037	0.030	–			
20	*A. poporum*	967B8	0.078	0.078	0.078	0.078	0.078	0.078	0.085	0.085	0.075	0.075	0.084	0.089	0.046	0.046	0.018	0.021	0.020	0.014	0.018	–		
21	*A. poporum*	967G9	0.078	0.078	0.078	0.078	0.078	0.078	0.085	0.085	0.075	0.075	0.084	0.089	0.046	0.046	0.018	0.021	0.020	0.014	0.018	0.000	–	
22	*A. poporum*	968B7	0.078	0.078	0.078	0.078	0.078	0.078	0.085	0.085	0.075	0.075	0.084	0.089	0.046	0.046	0.018	0.021	0.020	0.014	0.018	0.000	0.000	–
23	*A. poporum*	121E10	0.078	0.078	0.078	0.078	0.078	0.078	0.085	0.085	0.075	0.075	0.084	0.089	0.046	0.046	0.018	0.021	0.020	0.014	0.018	0.000	0.000	0.000

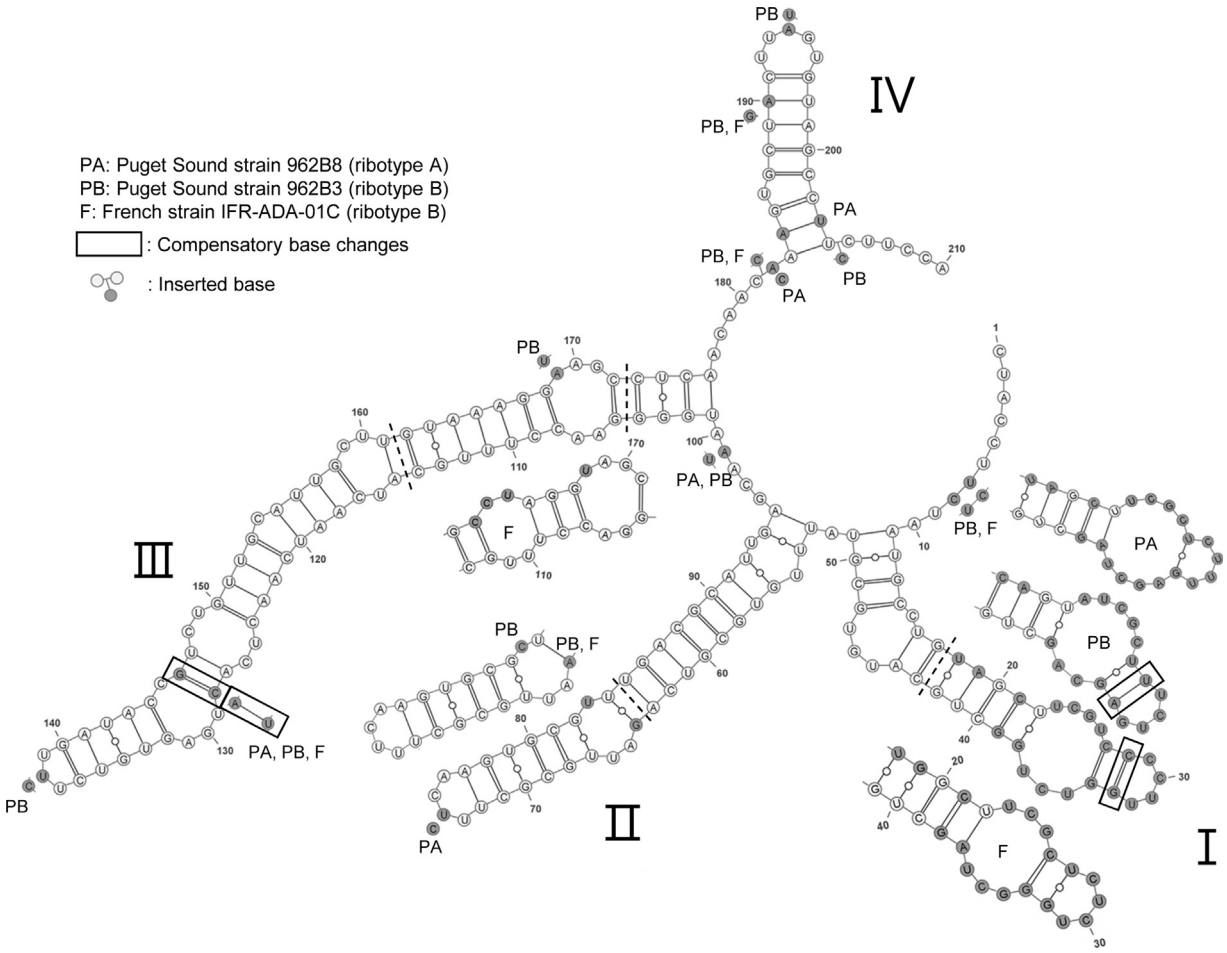

Fig. 5. Secondary structure of the ITS2 region of rRNA for Azadinium dalianense (AZCH02; China, ribotype A). The single base and stem-loop structure changes (dashed lines) are shown for the Puget Sound strains 962B8 (ribotype A), 962B3 (ribotype B) and the French strain IFR-ADA-01C (ribotype B), labeled as PA, PB and F, respectively. A shaded circles indicates a base change in 1 of the strains while an open circle indicates that the base is the same in all strains. Inserted bases (see legend) are present in ribotype B strains, but not in ribotype A. Compensatory base changes are marked with black boxes.

S121E10) showed the precursor mass *m/z* 860 of the fragment *m/z* 362, indicating the presence of a putative novel AZA. The collision induced dissociation (CID) spectrum of *m/z* 860 revealed a typical AZA spectrum displaying the characteristic group 3 to 5 fragments (Krock et al., 2012) *m/z* 262, 362 and 462 (Fig. 6A). Furthermore, the CID spectrum of *m/z* 860 was characterized by a group 2 fragment shifted to higher masses (*m/z* 700) in comparison to AZA-1 (*m/z* 672) and a very complex group 1 fragment cluster that does not

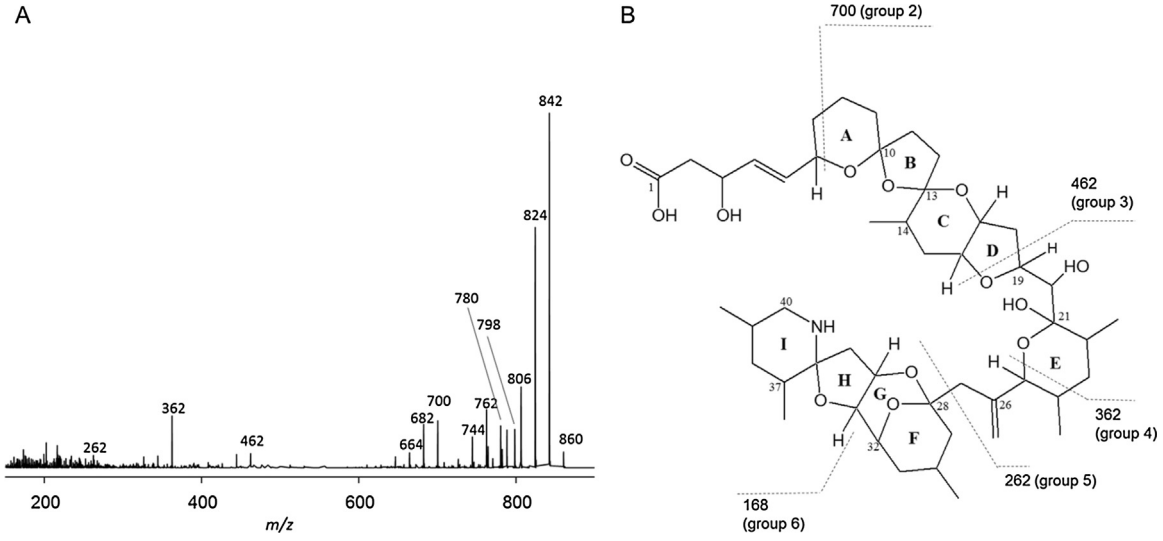

Fig. 6. (A) Collision induced dissociation (CID) spectrum of *m/z* 860 (AZA-59). (B) Proposed planar structure of AZA-59 and characteristic fragmentation sites with their respective *m/z* values.

only consist of several water losses from the pseudo-molecular ion (*m/z* 842, 824, 806 and 798) but also a CO_2 loss followed by several water losses (*m/z* 798, 780, 762 and 744). In addition to AZA-59, the corresponding phosphate derivative (*m/z* 940) was also detected (data not shown).

Cell quota of AZA-59 for the *A. poporum* strains was quite variable and ranged from 3.5 to 105.6 fg cell^{-1} (Suppl. Table S4). Independently grown subcultures of a given strain also varied in their AZA-59 cell quotas (Suppl. Table S4). Cellular amounts of AZA-59 phosphate were always less than 0.5% of AZA-59.

3.5. Selected reaction monitoring (SRM) analysis of SPATT samples

Fig. 7A illustrates a representative ion chromatogram from a neat calibration solution of AZA-1, -2 and -3 at 10 ng mL^{-1}. AZA-1, -2 and -3 were not detected in any of the SPATT resin extracts, but AZA-59 was detected at a retention time of approximately 4.5 min in both an *A. poporum* culture from Puget Sound and several SPATT samples (Fig. 7). Extracted ion chromatograms from the cell pellet and the SPATT sample from the 2014 Glen Ayr collection station are depicted in Fig. 7B and C, respectively. Fig. 1 and Table 3 summarize the detection results and concentration of AZA-59 measured in SPATT samples collected in 2014 and 2015, and include DTX-1 and OA concentrations for comparison. DTX-2 was not detected in any samples. Concentrations of AZA-59 were higher in 2014 relative to 2015, when only trace levels of this toxin were detected. The highest concentration of 2.7 ng AZA-59 per g resin was detected at Glen Ayr in 2014 (Fig. 1A, Table 3).

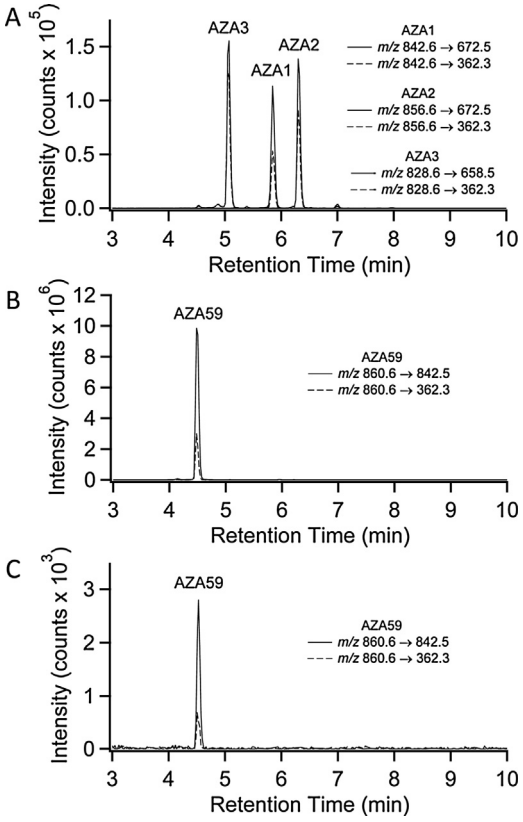

Fig. 7. Extracted ion chromatograms for (A) the separation of AZA-1, AZA-2 and AZA-3 in a neat calibration solution at 10 ng mL^{-1}, (B) AZA-59 from *Azadinium poporum* (121E10) culture from Puget Sound and (C) AZA-59 from SPATT resin deployed at the Glen Ayr station in July 2014. The transitions monitored for quantitation and confirmation are displayed as solid and dashed lines, respectively.

Table 3
Concentrations of DSTs and AZA in SPATT Extracts in 2014 and 2015.

2014	July			August		
NOAA Sample Name	AZA-59*	DTX-1*	OA*	AZA-59*	DTX-1*	OA*
Birch Bay	ND	11.5	ND	ND	13.9	ND
Cornet Bay	ND	Trace	ND	ND	11.0	ND
Des Moines	ND	ND	ND	ND	6.3	ND
Discovery Bay	ND	64.0	ND	ND	120.7	ND
Ediz Hook	ND	Trace	ND	ND	35.6	Trace
Edmonds	Trace	ND	ND	ND	Trace	ND
Fort Worden	ND	Trace	ND	ND	Trace	ND
Friday Harbor	ND	Trace	ND	ND	50.6	ND
Glen Ayr	2.7	11.8	ND	0.6	5.2	ND
Manchester Bay	0.9	31.3	ND	ND	12.2	ND
Mystery Bay	ND	66.5	ND	ND	Trace	ND
North Bay-Allyn	ND	Trace	ND	ND	8.1	Trace
Oakland Bay	ND	Trace	ND	ND	Trace	ND
Penn Cove	ND	ND	ND	Trace	Trace	ND
Penrose Point Park	ND	ND	ND	ND	Trace	ND
Pleasant Harbor	1.0	Trace	ND	ND	Trace	ND
Port Susan	–	–	–	Trace	Trace	ND
Quartermaster Harbor	ND	Trace	ND	ND	96.2	ND
Sequim Bay I	ND	50.2	ND	ND	119.7	Trace
Sequim Bay II	ND	84.2	Trace	ND	198.4	Trace
Squalicum Harbor	ND	38.5	ND	ND	30.8	ND
Tokeland	ND	35.4	ND	ND	23.8	ND
Westport	ND	47.4	Trace	ND	14.5	ND
Zittel's Marina	–	–	–	ND	10.8	ND
2015	**July**			**August**		
Birch Bay	ND	1.5	ND	ND	5.3	ND
Burley Lagoon	ND	8.0	ND	ND	7.8	ND
Cornet Bay	ND	3.7	Trace	–	–	–
Des Moines	ND	17.7	1.6	ND	4.6	ND
Discovery Bay	–	–	–	ND	24.6	1.8
Ediz Hook	–	–	–	ND	6.4	1.5
Edmonds	ND	5.2	Trace	ND	9.9	Trace
Fort Worden	ND	8.3	Trace	ND	6.7	1.6
Manchester Bay	Trace	24.6	Trace	ND	22.4	1.7
Mystery Bay	ND	2.7	ND	ND	3.9	ND
North Bay-Allyn	ND	44.0	3.5	Trace	21.8	2.7
Oakland Bay	ND	18.1	Trace	ND	23.1	2.3
Penn Cove	Trace	4.6	ND	–	–	–
Penrose Point Park	ND	8.7	Trace	ND	8.2	ND
Pleasant Harbor	ND	11.6	Trace	ND	5.4	ND
Port Gamble	ND	16.6	ND	–	–	–
Port Susan	–	–	–	Trace	122.9	18.8
Quartermaster Harbor	ND	8.2	ND	ND	13.1	ND
Quilcene Bay	ND	9.7	Trace	Trace	5.6	ND
Sequim Bay I	–	–	–	ND	12.7	Trace
Sequim Bay II	–	–	–	ND	17.3	ND
Squalicum Harbor	ND	7.4	ND	ND	6.0	ND
Tokeland	ND	7.2	ND	ND	7.4	ND
Westport	ND	12.1	Trace	ND	6.2	ND
Zittel's Marina	ND	6.2	ND	–	–	–

* = Toxin unit is ng·g^{-1} resin.
ND = Not Detected, Quantitation Ion S/N < 10 or Quantitation and Confirmatory Ion S/N < 3.
Trace = Quantitation Ion S/N ≥ 10 and Confirmatory Ion < 3, or Quantitation and Confirmatory Ion S/N ≥ 3.
– = No Sample.

4. Discussion

4.1. Diversity of Azadinium in Puget Sound

The genus *Azadinium* has been of interest after the initial discovery of AZA-1 production by *A. spinosum* (Krock et al., 2009; Tillmann et al., 2009), a finding that required over 10 years of study after the first human poisonings by this toxin were recognized. Records of *Azadinium* spp. have extended to Europe, Northeast Asia and Oceania (Potvin et al., 2012; Tillmann et al., 2014a; Smith et al., 2015). For the American continent, their presence recently has been confirmed in the Gulf of Mexico (Luo et al., 2016), in the

Southwest Atlantic region of Argentina (Tillmann et al., 2016) and in the Southeast Pacific region of Chile (Tillmann et al., 2017b). In the Northeast Pacific region of America, *Azadinium* had been detected only by molecular techniques (Adams et al., in prep.) and low levels of AZA-2 in plankton samples have been described (Trainer et al., 2013). In attempt to fully describe the diversity and toxin production potential of *Azadinium* in the Puget Sound region, *Azadinium* were isolated from sediment samples and analyzed using morphologic, molecular and chemical analyses. The qPCR prescreening method using both specific *Azadinium* and general Amphidomataceae probes assisted in selecting stations for sediment incubation. Isolation of cells by sediment incubation was attempted at more than 10 stations (Fig. 1, not all stations are shown), but *Azadinium* were obtained only from sediment collected at Dabob Bay and Center Lynch Cove. This is consistent with the qPCR analysis that indicated a relatively low abundance of *Azadinium* for the other stations. Therefore, when trying to obtain *Azadinium* cultures from sediment incubation, qPCR prescreening using specific and/or a general Amphidomataceae probes can greatly improve success.

The possibility that other *Azadinium* species (e.g., the toxigenic *A. spinosum*) could be present in Puget Sound waters cannot be excluded. In fact, *A. spinosum* likely is present, as preliminary tests using species specific primers (Toebe et al., 2013) yielded positive signals for all three species, *A. obsesum*, *A. poporum* and *A. spinosum* (Adams et al., in prep). The present work is a first step to the full description of Amphidomataceae diversity in the region.

Although *Azadinium* vegetative cells were successfully obtained from sediments, this study has not yet been able to identify and characterize *Azadinium* cysts, likely due to their small size. Previous successful sediment incubation experiments obtaining *Azadinium* species (Luo et al., 2013, 2017; Potvin et al., 2012) suggest that a resting stage is likely for *A. poporum*, *A. dalianense* and *A. zhuanum*. Cyst-like stages have been described from a culture of *A. polongum* (Tillmann et al., 2012b). This study now add *A. cuneatum* and *A. obesum* to the list of Amphidomatacean species likely to have a resting stage.

Based on the morphological and phylogenetic characterization presented here, at least 4 different *Azadinium* species are present in Puget Sound. The presence of *Azadinium obesum* and *A. cuneatum* have only been reported from the Scottish coast (Tillmann et al., 2010) and from the Irminger Sea (Tillmann et al., 2014a), respectively. The Northeast Pacific record thus represents an important range extension of these two species. In terms of morphology, the North Pacific strains of both species conform to their Atlantic counterparts. As has been described for the type strain of *A. obesum,* both configurations of the central epithecal intercalary plate (5-sided or 4-sided) were observed in the *A. obesum* strain 481F2 from Puget Sound. Such intraspecific variability of Plate 2a configuration is also documented for the type culture of *A. cuneatum* (Tillmann et al., 2014a) and field populations of *A. luciferelloides* (Tillmann and Akselman, 2016) and thus probably is widespread among *Azadinium* species. Furthermore, all new strains of these two species do not produce AZA, which supports evidence from other geographical regions that both species are non-AZA producers. Nucleotide sequences of ITS1-5.8S-ITS2 and LSU regions of Northeast Pacific strains of *A. obesum* (1 bp deletion in the ITS region and 4 bp substitutions in the partial LSU sequence) and *A. cuneatum* (only 1 bp difference in the partial LSU sequence) are almost identical to those of the North Atlantic. This suggests that recent uninhibited gene flow of *Azadinium* between the Northeast Pacific and Arctic North Atlantic waters may have occurred, causing currents to connect the two regions and allow cysts or vegetative cells to travel through the North Pole region (Reid et al., 2007; Scholin et al., 1995).

Luo et al. (2013) first described *Azadinium dalianense* from China, but a new strain recently obtained from the French Atlantic (Luo et al., 2017) already indicated that this species probably also has a wide distribution. This notion is confirmed here with the first record of the species from the Northeast Pacific. As it is the case for *A. cuneatum* and *A. obesum*, the lack of AZA in the new Puget Sound *A. dalianense* strains confirm previous reports on the lack of toxigenicity of the Chinese and French *A. dalianese* strains (Luo et al., 2013, 2017). Molecular phylogeny, however, show that sequence variability among *A. dalianense* strains from different areas, but also among strains from Puget Sound, can be substantial and are significantly larger than among different strains of *A. obesum* and *A. cuneatum* as discussed above. Compared to the Chinese strain AZCH02, strain 962B8, for example, is different in the ITS region with a *p*-distance of 0.027 (Table 4), but nevertheless both strains belong to one cluster in the phylogenetic tree (Fig. 4). Strain 962B3 is even more divergent from AZCH02 and in the phylogenetic tree shares the same distinct clade as the French strain. These two distinct *A. dalianense* clades are designated here as ribotype A and B, respectively. In particular, the ITS region *p*-distance of the Chinese strain AZCH02 (ribotype A) and Puget Sound strain 962B3 (ribotype B) was as large as 0.062. This is greater than 0.046, the minimum *p*-distance between the *Azadinium* species, *A. obesum* and *A. poporum* determined here (Table 2) and higher than a general ITS sequence data based threshold of 0.04 proposed by Litaker et al. (2007) to differentiate between a single and different species. Amphidomataceae, however, may have larger intragenomic variability compared to other dinoflagellates, as high intragenomic ITS *p*-distances (0.045) for a strain of *Am. languida* (Tillmann et al., 2017a), and between two individual strains of *A. dexteroporum* (0.04) have been reported (Tillmann et al., 2015). Detailed morphological investigation of the new Puget Sound *A. dalianense* strains show that they have the same cell size, shape, pyrenoid location and plate pattern as described previously for two other *A. dalianense* strains from China (Luo et al., 2013) and from the French Atlantic (Luo et al., 2017). There are, however, indications that the frequency of the presence of an antapical spine located at Plate 2′′′′ might be different among strains. The *A. dalianense* type culture strain AZCH02 (designated here as ribotype A) from China had a spine in 18% of the cells (Luo et al., 2013). In contrast, for the French strain (ribotype B), it is reported that all cells in culture had a spine (Luo et al., 2017). All four *A. dalianense* strains obtained from Puget Sound had a higher proportion of cells with a spine than the Chinese strains, even those strains (962B8 and 121F6) that share the same ribotype with strain AZCH02 (Table 1, Suppl. Figs. S6, S7). Both 962B8 and 121F6 had large differences in nucleotide sequence compared to the Chinese strain (AZCH02), and were close to ribotype B (Fig. 4), indicating that spine frequency might serve as a proxy for a ribotype designation. Nevertheless, future research is needed to more clearly describe this inter-strain variability in spine formation. Moreover, a tendency was observed in Puget Sound ribotype B strains that the dorsal cingular Plate 4C for many cells was rather narrow (Suppl. Figs. S4, S5). All these morphological features were variable within the clonal cultures, so it can be concluded that currently no significant morphological difference within the ribotypes of *A. dalianense* can be deciphered which would justify proposing separate species. On the molecular level, however, the ITS2 secondary structure analysis among *A. dalianense* strains revealed the presence of compensatory base pair changes (CBCs), which generally are discussed as a criterion for distinguishing species (Müller et al., 2007; Wolf et al., 2013). The presence of CBCs in the conserved region of helix III (5′-side 30 bp from tip of helix III) is known to correlate with a decrease in gamete compatibility (Coleman, 2009). In this conserved region of helix III, CBCs were observed between strain AZCH02 (ribotype A) and 962B3, IFR-

ADA-01C (ribotype B), but also between AZCH02 and 962B8 that share the same ribotype. There were no CBCs among 962B8 (ribotype A) and the ribotype B strains (962B3, IFR-ADA-01C). Thus, while Puget Sound ribotype A strain (962B8) clustered with Chinese ribotype A (AZCH02) in the phylogenetic tree, its ITS2 secondary structure is more closed to ribotype B strains. More *A. dalianense* strains from different global regions thus are needed to refine the evolutionary relationship within *A. dalianense* to determine whether reproductive segregation between strains of *A. dalianense* is actually present (which would make a taxonomic revision of this species necessary). This would require breeding experiments, which in turn require a basic understanding of the yet unresolved sexual cycle of *Azadinium*.

The four *A. poporum* strains identified from Puget Sound did not differ in morphology from *A. poporum* from other areas (Tillmann et al., 2011, 2016; Luo et al., 2016). This includes the presence of a field of pores on the large antapical Plate 2′′′′ that was also recently described for strains from Argentina (Tillmann et al., 2016) and the Gulf of Mexico (Luo et al., 2016). In terms of sequence data, the Northeast Pacific strains share the same ribotype as strains from the South Pacific (Chile), the European North Atlantic, New Zealand (LSU only available in gene bank), and a recently added strain from the Mediterranean Sea. Sequence data thus indicate that there might be dispersal links between these distant geographical areas.

All four strains of *A. poporum* from Puget Sound produced AZA-59 as the sole AZA, adding to the notion that the AZA profile of *A. poporum* is quite diverse. Strains from the South Pacific (Chile) produce AZA-11 (Tillmann et al., 2017b), strains from the West Atlantic (Argentina, Gulf of Mexico) and from the Mediterranean produce AZA-2 (Tillmann et al., 2016; Luo et al., 2017), strains from Europe produce AZA-37 (Krock et al., 2012), and in strains from Asia, a large number of AZA (AZA-2, -11, -36, -40, -41) were found (Krock et al., 2014). With now more than 40 strains obtained from various areas, *A. poporum* seems to be the most widespread and abundant species of the genus, and the current record from the Northwest Pacific contributes to the records from the northeast Atlantic (Tillmann et al., 2011), southwest Atlantic (Tillmann et al., 2016), southeast Pacific (Tillmann et al., 2017b) and southwest Pacific (Potvin et al., 2012). Cell quotas of AZA-59 estimated here are well within or above the range of ~5–20 fg cell^{-1} often reported for other AZA producing species (Tillmann et al., 2014b). Variability in AZA cell quota within the Puget Sound strains likely reflects the variable accumulation of secondary metabolites in dense cultures during stationary phase. Clearly, more detailed laboratory experiments will define the environmental effects on AZA cell quota in Puget Sound *A. poporum*.

4.2. Identification of a novel AZA

The presence of a yet unreported azaspiracid in the four *A. poporum* strains with the pseudo-molecular mass of *m/z* 860 was verified by its characteristic AZA collision-induced dissociation (CID) spectrum. Since the group 3 to 5 fragments (*m/z* 462, 362 and 262) are identical with those of AZA-1, a conserved structure between both compounds can be assumed, i.e. the N-containing part of the molecule including C19 to C40. On the other hand, there are some pronounced differences between AZA-1 and the new compound, which consist in a shift to higher masses of the group 2 fragment cluster and the CO_2 loss from the pseudo-molecular ion that both are not observed in the CID spectrum of AZA-1. Both characteristics appear in the CID spectrum of AZA-37 (compound 2 in Krock et al., 2012) that posteriorly was identified as 3-hydroxy-7,8-dihydro-39-demethyl-azaspiracid-1 (Krock et al., 2015) by nuclear magnetic resonance (NMR) spectroscopy. In fact, the CID spectrum of AZA-37 produced by *A. poporum* isolates from the North Sea is identical to the CID spectrum of *A. poporum* from the Puget Sound with the exception that all group 1–5 fragments are shifted to 14 Da higher masses, indicating an additional methyl group in the new AZA in comparison to AZA-37. But since the new AZA has identical group 3–5 fragments as AZA-1, it is very reasonable to assume that the methyl group is located at C39 as in most AZAs. Taken together, these pieces of evidence demonstrate a novel AZA with the putative structure 3-hydroxy-7,8-dihydro-azaspiracid-1 (Fig. 6B). The name AZA-59 is proposed for this novel AZA in line with the chronological AZA numbering. In this work, structural assignment was based solely on mass spectral data; for confirmation, additional sample material will be required for NMR spectroscopy.

In addition to AZA-59, small amounts of AZA-59 phosphate were detected in the *A. poporum* strains from Puget Sound. This finding is not surprising since the respective AZA phosphates have been detected in strains of *A. poporum* from other geographic locations as well. AZA-2 phosphate was detected in *A. poporum* strains from the Argentine shelf margin (Tillmann et al., 2016) and AZA-11 phosphate in strains from the northern Chilean Pacific coast (Tillmann et al., 2017b). These findings indicate that the formation of AZA phosphates may be a common feature among *A. poporum*. In any case, as it has been reported for other *A. poporum* strains, the AZA-59 phosphate in all four Puget Sound strains was a minor compound amounting for <0.5% of AZA-59.

This study does not provide any data on the toxicity of AZA-59, as reliable toxicity testing requires purified compounds. The respective mass culturing and purification work for Puget Sound *A. poporum* compounds is beyond the scope of the present study and currently is in progress. In any case, because AZA-59 is almost identical to AZA-37 (Krock et al., 2015), with an additional methyl group at C39 in AZA-59 as the only difference, it might be assumed that the toxicity of these 2 toxin congeners will be similar. Using a T lymphocyte cell viability assay, purified AZA-37, with a 24 h EC_{50} of 0.91 nM, was found to be approximately 3-fold less potent than AZA-1 (Krock et al., 2015). Once purified AZA-59 is available, tests to determine its toxicity equivalency compared to AZA-1, -2, and -3 are planned.

4.3. AZA in SPATT

A “shotgun” approach was used to deploy SPATT samplers in 2014 and 2015 at multiple locations in Puget Sound as well as two stations on the outer WA State coast, and these samples were used retrospectively to confirm the *in situ* presence of AZA-59. The majority of stations where SPATT samplers were deployed were negative for AZA-59. Eight stations, including three in Hood Canal – Quilcene Bay, Pleasant Harbor and Glen Ayr – and five in the main basin of Puget Sound – Port Susan, Edmonds, Penn Cove, Manchester Bay and North Bay-Allyn – were positive for AZA-59.

As AZA-59 has not yet been reported in shellfish, it is difficult at present to assess the risks for this toxin on human health. For comparison, SPATT samples were also analyzed for DSTs, which are known to occur in shellfish in excess of regulatory safety levels and cause shellfish harvesting closures in the Puget Sound region. No correlations were observed between levels of AZA-59 and levels of DSTs on SPATT resin. At Glen Ayr, the highest concentration of AZA-59 was detected at 2.7 ng g^{-1} resin, while the concentration of DTX-1 at this station was 11.8 ng g^{-1} resin. During the period when SPATT samplers were deployed, DST concentrations in mussels at Glen Ayr were detectable at only 1 μg 100 g^{-1} (Washington State Department of Health, pers. comm.), well below the regulatory threshold of 16 μg 100 g^{-1} shellfish. In contrast, levels of DSTs on SPATT resin in August 2014 ranged from 100 to 200 ng g^{-1} at the Sequim Bay sampling stations, while AZA-59 was not detected. In 2011, during the first shellfish harvesting closures in the state,

shellfish from this area reached 160.3 μg 100 g^{-1} and have exceeded regulatory guidance levels in this region several times since that time (Lloyd et al., 2013; Trainer et al., 2013; Washington State Department of Health, Marine Biotoxin database). Future studies are planned where SPATT will be deployed at select high priority sites in Puget Sound and used to prioritize the analysis of shellfish for AZA-59.

5. Conclusions

Four species of *Azadinium* were isolated from Puget Sound sediment, including *A. cuneatum, A. obesum, A. dalianense* and *A. poporum*. A new toxin, named AZA-59, was identified and characterized in four *A. poporum* isolates while none of the known azaspiracids, as determined by LC–MS/MS, were found in the other *Azadinium* species isolated from the Pacific Northwest. A solid phase resin, deployed for 1-week periods at several stations in Puget Sound and on the outer Washington State coast, showed the presence of AZA-59 at 8 stations.

Establishing clonal cultures of *Azadinium* is a straightforward tool that was used to clarify the diversity and potential toxicity of *Azadinium* species. The results show that various non AZA-producing species (*A. obesum*, *A. cuneatum* and *A. dalianense*) co-occurred in the area with the AZA-producing *A. poporum*. All these species are very similar in size and shape and difficult to identify by light microscope, thus any microscopic alerts of the presence of "*Azadinium*-like" species in field samples require confirmation by more detailed SEM and/or molecular based investigations. The establishment of cultures enabled the detection of a new AZA structural variant as the sole AZA produced by local *A. poporum* strains and thus allowed to refine the detection methods and to specifically monitor the presence and concentration of this compound. The combined strategy of sediment and whole water sampling for species using molecular identification as well as solid phase resin deployment will be used in the future pinpoint locations where the risk of toxins in shellfish is greatest.

Acknowledgements

We thank Brian Bill for assistance with SEM. We thank Cheryl Greengrove, Julie Masura, and the captain and crew of the R/V Clifford A. Barnes for 2016 cruise sampling. We thank SoundToxins participants and other volunteers for their help with SPATT sampling, including Jerry Borchert, Clara Hard, Dana Woodruff, Ewann Berntson, Franchesca Perez, Jamie Landry, Jennifer Runyan, Joanna Harrison, Karlista Rickerson, Olivia Graham, Sarah Whitten, Rory O'Rourke, Linda Rhodes, Maggie Taylor, Neil Harrington, Sandy Wyllie-Echeverria, Sue Shotwell, Teri King, Tim Jones, Zach Forster, Nicole Hamlin, Justin Lanman, Claire Chisholm and Natalie Sahli. We thank Shailesh Patidar for assistance with editing the paper. This research was supported in part by a grant from the NOAA National Centers for Coastal Ocean Science's Monitoring and Event Response to Harmful Algal Blooms (MERHAB) program and supported by Basic Science Research Program through the National Research Foundation of Korea (NRF) funded by the Ministry of Science, ICT and future Planning (NRF-2015R1A2A2A01008115). Partial financial support was also provided by the PACES research program of the Alfred Wegener Institute as part of the Helmholtz Foundation initiative in Earth and Environment. This is MERHAB publication #200. [CG]

Appendix A. Supplementary data

Supplementary data associated with this article can be found, in the online version, at http://dx.doi.org/10.1016/j.hal.2017.08.004.

References

Coleman, A.W., 2009. Is there a molecular key to the level of biological species in eukaryotes? A DNA guide. Mol. Phylogenet. Evol. 50 (1), 197–203.
Craib, J., 1965. A sampler for taking short undisturbed marine cores. Journal du Conseil 30 (1), 34–39.
Darty, K., Denise, A., Ponty, Y., 2009. VARNA: Interactive drawing and editing of the RNA secondary structure. Bioinformatics 25 (15), 1974–1975.
Flanagan, A.F., Callanan, K.R., Donlon, J., Palmer, R., Forde, A., Kane, M., 2001. A cytotoxicity assay for the detection and differentiation of two families of shellfish toxins. Toxicon 39 (7), 1021–1027.
Fux, E., Bire, R., Hess, P., 2009. Comparative accumulation and composition of lipophilic marine biotoxins in passive samplers and in mussels (*M. edulis*) on the West Coast of Ireland. Harmful Algae 8 (3), 523–537.
Gu, H.F., Luo, Z.H., Krock, B., Witt, M., Tillmann, U., 2013. Morphology: phylogeny and azaspiracid profile of *Azadinium poporum* (Dinophyceae) from the China Sea. Harmful Algae 21-22, 64–75.
Hall, T.A., 1999. BioEdit: a user-friendly biological sequence alignment editor and analysis program for Windows 95 /98/NT. Nucleic Acids Symp. Ser. 95–98.
Harrison, P.J., Waters, R.E., Taylor, F., 1980. A broad spectrum artificial sea water medium for coastal and open ocean phytoplankton. J. Phycol. 16 (1), 28–35.
Huelsenbeck, J.P., Ronquist, F., 2001. MRBAYES: Bayesian inference of phylogenetic trees. Bioinformatics 17 (8), 754–755.
James, K.J., Furey, A., Lehane, M., Ramstad, H., Aune, T., Hovgaard, P., Morris, S., Higman, W., Satake, M., Yasumoto, T., 2002. First evidence of an extensive northern European distribution of azaspiracid poisoning (AZP) toxins in shellfish. Toxicon 40 (7), 909–915.
Keller, A., Schleicher, T., Schultz, J., Müller, T., Dandekar, T., Wolf, M., 2009. 5.8 S-28S rRNA interaction and HMM-based ITS2 annotation. Gene 430 (1), 50–57.
Kim, J.-H., Kim, J., Wang, P., Park, B., Han, M.-S., 2015. An improved quantitative real-time pcr assay for the enumeration of *Heterosigma akashiwo* (Raphidophyceae) cysts using a DNA debris removal method and a cyst-based standard curve. PLoS One 11 (1), e0145712.
Kilcoyne, J., Nulty, C., Jauffrais, T., McCarron, P., Herve, F., Foley, B., Rise, F., Crain, S., Wilkins, A.L., Twiner, M.J., Hess, P., Miles, C.O., 2014. Isolation, structure elucidation, relative LC-MS response, and in vitro toxicity of azaspiracids from the dinoflagellate *Azadinium spinosum*. J. Nat. Prod. 77 (11), 2465–2474.
Kilcoyne, J., Twiner, M.J., McCarron, P., Crain, S., Giddings, S.D., Foley, B., Rise, F., Hess, P., Wilkins, A.L., Miles, C.O., 2015. Structure elucidation, relative LC–MS response and in vitro toxicity of Azaspiracids 7–10 isolated from mussels (*Mytilus edulis*). J. Agric. Food Chem. 63 (20), 5083–5091.
Krock, B., Tillmann, U., John, U., Cembella, A.D., 2009. Characterization of azaspiracids in plankton size-fractions and isolation of an azaspiracid-producing dinoflagellate from the North Sea. Harmful Algae 8 (2), 254–263.
Krock, B., Tillmann, U., Voß, D., Koch, B.P., Salas, R., Witt, M., Potvin, É., Jeong, H.J., 2012. New azaspiracids in *Amphidomataceae* (Dinophyceae). Toxicon 60 (5), 830–839.
Krock, B., Tillmann, U., Witt, M., Gu, H.F., 2014. Azaspiracid variability of *Azadinium poporum* (Dinophyceae) from the China sea. Harmful Algae 36, 22–28.
Krock, B., Tillmann, U., Potvin, É., Jeong, H.J., Drebing, W., Kilcoyne, J., Al-Jorani, A., Twiner, M.J., Göthel, Q., Köck, M., 2015. Structure elucidation and *in vitro* toxicity of new azaspiracids isolated from the marine dinoflagellate *Azadinium poporum*. Mar. Drugs 13 (11), 6687–6702.
Kumar, S., Stecher, G., Tamura, K., 2016. MEGA7: molecular evolutionary genetics analysis version 7.0 for bigger datasets. Mol. Biol. Evol. 33 (7), 1870–1874.
López-Rivera, A., O'Callaghan, K., Moriarty, M., O'Driscoll, D., Hamilton, B., Lehane, M., James, K.J., Furey, A., 2010. First evidence of azaspiracids (AZAs): A family of lipophilic polyether marine toxins in scallops (*Argopecten purpuratus*) and mussels (*Mytilus chilensis*) collected in two regions of Chile. Toxicon 55 (4), 692–701.
Litaker, R.W., Vandersea, M.W., Kibler, S.R., Reece, K.S., Stokes, N.A., Lutzoni, F.M., Yonish, B.A., West, M.A., Black, M.N.D., Tester, P.A., 2007. Recognizing dinoflagellate species using ITS rDNA sequences. J. Phycol. 43 (2), 344–355.
Lloyd, J.K., Duchin, J.S., Borchert, J., Quintana, H.F., Robertson, A., 2013. Diarrhetic shellfish poisoning, Washington, USA, 2011. Emerg. Infect. Dis. 19 (8), 1314–1316.
Luo, Z., Gu, H., Krock, B., Tillmann, U., 2013. *Azadinium dalianense*, a new dinoflagellate species from the Yellow Sea, China. Phycologia 52 (6), 625–636.
Luo, Z., Krock, B., Mertens, K.N., Price, A.M., Turner, R.E., Rabalais, N.N., Gu, H., 2016. Morphology, molecular phylogeny and azaspiracid profile of *Azadinium poporum* (Dinophyceae) from the Gulf of Mexico. Harmful Algae 55, 56–65.
Luo, Z., Krock, B., Mertens, K.N., Nézan, E., Chomérat, N., Bilien, G., Tillmann, U., Gu, H., 2017. Adding new pieces to the Azadinium (Dinophyceae) diversity and biogeography puzzle: non-toxigenic *Azadinium zhuanum* sp. nov. from China, toxigenic *A. poporum* from the Mediterranean, and a non-toxigenic A. dalianense from the French Atlantic. Harmful Algae 66, 65–78.
Müller, T., Philippi, N., Dandekar, T., Schultz, J., Wolf, M., 2007. Distinguishing species. RNA 13 (9), 1469–1472.
McMahon, T., Silke, J., 1996. West coast of Ireland: winter toxicity of unknown aetiology in mussles. Harmful Algae News 14, 2.
Nézan, E., Tillmann, U., Bilien, G., Boulben, S., Chèze, K., Zentz, F., Salas, R., Chomérat, N., 2012. Taxonomic revision of the dinoflagellate *Amphidoma caudata*: transfer to the genus Azadinium (Dinophyceae) and proposal of two varieties, based on morphological and molecular phylogenetic analyses. J. Phycol. 48 (4), 925–939.

Percopo, I., Siano, R., Rossi, R., Soprano, V., Sarno, D., Zingone, A., 2013. A new potentially toxic Azadinium species (Dinophyceae) from the Mediterranean Sea, *A. dexteroporum* sp. nov. J. Phycol 49 (5), 950–966.

Potvin, É., Jeong, H.J., Kang, N.S., Tillmann, U., Krock, B., 2012. First report of the photosynthetic dinoflagellate genus *Azadinium* in the Pacific ocean: morphology and molecular characterization of *Azadinium cf. poporum*. J. Eukaryot. Microbiol. 59 (2), 145–156.

Reid, P.C., Johns, D.G., Edwards, M., Starr, M., Poulin, M., Snoeijs, P., 2007. A biological consequence of reducing Arctic ice cover: arrival of the Pacific diatom *Neodenticula seminae* in the North Atlantic for the first time in 800,000 years. Glob. Chang. Biol. 13 (9), 1910–1921.

Ronzitti, G., Hess, P., Rehmann, N., Rossini, G.P., 2007. Azaspiracid-1 alters the E-cadherin pool in epithelial cells. Toxicol. Sci. 95 (2), 427–435.

Rossi, R., Dell'Aversano, C., Krock, B., Ciminiello, P., Percopo, I., Tillmann, U., Soprano, V., Zingone, A., 2017. Mediterranean *Azadinium dexteroporum* (Dinophyceae) produces six novel azaspiracids and azaspiracid-35: a structural study by a multi-platform mass spectrometry approach. Anal. Bioanal. Chem. 409 (4), 1121–1134.

Rundberget, T., Gustad, E., Samdal, I.A., Sandvik, M., Miles, C.O., 2009. A convenient and cost-effective method for monitoring marine algal toxins with passive samplers. Toxicon 53 (5), 543–550.

Salas, R., Tillmann, U., John, U., Kilcoyne, J., Burson, A., Cantwell, C., Hess, P., Jauffrais, T., Silke, J., 2011. The role of *Azadinium spinosum* (Dinophyceae) in the production of azaspiracid shellfish poisoning in mussels. Harmful Algae 10 (6), 774–783.

Satake, M., Ofuji, K., Naoki, H., James, K.J., Furey, A., McMahon, T., Silke, J., Yasumoto, T., 1998. Azaspiracid, a new marine toxin having unique spiro ring assemblies, isolated from Irish mussels, *Mytilus edulis*. J. Am. Chem. Soc 120 (38), 9967–9968.

Scholin, C., Herzog, M., Sogin, M., Anderson, D., 1994. Identification of group-and strain-specific genetic markers for globally distributed *Alexandrium* (Dinophyceae). II. Sequence analysis of a fragment of the LSU rRNA gene. J. Phycol. 30 (6), 999–1011.

Scholin, C.A., Hallegraeff, G.M., Anderson, D.M., 1995. Molecular evolution of the *Alexandrium tamarense* 'species complex' (Dinophyceae): dispersal in the north american and west pacific regions. Phycologia 34 (6), 472–485.

Seibel, P.N., Müller, T., Dandekar, T., Schultz, J., Wolf, M., 2006. 4SALE–a tool for synchronous RNA sequence and secondary structure alignment and editing. BMC Bioinf. 7 (1), 1.

Smith, K.F., Rhodes, L., Harwood, D.T., Adamson, J., Moisan, C., Munday, R., Tillmann, U., 2015. Detection of *Azadinium poporum* in New Zealand: the use of molecular tools to assist with species isolations. J. Appl. Phycol. 1–8.

Taleb, H., Vale, P., Amanhir, R., Benhadouch, A., Sagou, R., Chafik, A., 2006. First detection of azaspiracids in mussels in north west Africa. J. Shellfish Res. 25 (3), 1067–1070.

Thompson, J.D., Higgins, D.G., Gibson, T.J., 1994. Clustal-W – Improving the sensitivity of progressive multiple sequence alignment through sequence weighting, position-specific gap penalties and weight matrix choice. Nucleic Acids Res. 22 (22), 4673–4680.

Tillmann, U., Akselman, R., 2016. Revisiting the 1991 algal bloom in shelf waters off Argentina: *Azadinium luciferelloides* sp. nov. (Amphidomataceae, Dinophyceae) as the causative species in a diverse community of other amphidomataceans. Phycol. Res. 64 (3), 160–175.

Tillmann, U., Elbrächter, M., Krock, B., John, U., Cembella, A., 2009. *Azadinium spinosum* gen. et sp. nov. (Dinophyceae) identified as a primary producer of azaspiracid toxins. Eur. J Phycol. 44 (1), 63–79.

Tillmann, U., Elbrächter, M., John, U., Krock, B., Cembella, A., 2010. *Azadinium obesum* (Dinophyceae), a new nontoxic species in the genus that can produce azaspiracid toxins. Phycologia 49 (2), 169–182.

Tillmann, U., Elbrächter, M., John, U., Krock, B., 2011. A new non-toxic species in the dinoflagellate genus *Azadinium*: *A. Poporum* sp. nov. Eur. J. Phycol. 46 (1), 74–87.

Tillmann, U., Salas, R., Gottschling, M., Krock, B., O'Driscoll, D., Elbrächter, M., 2012a. *Amphidoma languida* sp. nov. (Dinophyceae) reveals a close relationship between *Amphidoma* and *Azadinium*. Protist 163 (5), 701–719.

Tillmann, U., Soehner, S., Nézan, E., Krock, B., 2012b. First record of the genus *Azadinium* (Dinophyceae) from the Shetland Islands: including the description of *Azadinium polongum* sp. nov. Harmful Algae 20, 142–155.

Tillmann, U., Gottschling, M., Nézan, E., Krock, B., Bilien, G., 2014a. Morphological and molecular characterization of three new *Azadinium* species (Amphidomataceae, dinophyceae) from the Irminger sea. Protist 165 (4), 417–444.

Tillmann, U., Salas, R., Jauffrais, T., Hess, P., Silke, J., 2014b. AZA: The producing organisms—Biology and trophic transfer, Seafood and Freshwater Toxins, Pharmacology, Physiology, and Detection. 3rd ed. Taylor & Francis, pp. 773–798.

Tillmann, U., Gottschling, M., Nézan, E., Krock, B., 2015. First records of *Amphidoma languida* and *Azadinium dexteroporum* (Amphidomataceae, dinophyceae) from the irminger sea off Iceland. Mar. Biodivers. Rec. 8, e142.

Tillmann, U., Borel, C.M., Barrera, F., Lara, R., Krock, B., Almandoz, G.O., Witt, M., Trefault, N., 2016. *Azadinium poporum* from the Argentine Continental Shelf, Southwestern Atlantic, produces azaspiracid-2 and azaspiracid-2 phosphate. Harmful Algae 51, 40–55.

Tillmann, U., Jaen, D., Fernández, L., Gottschling, M., Witt, M., Blanco, J., Krock, B., 2017a. *Amphidoma languida* (Amphidomatacea, Dinophyceae) with a novel azaspiracid toxin profile identified as the cause of molluscan contamination at the Atlantic coast of southern Spain. Harmful Algae 62, 113–126.

Tillmann, U., Trefault, N., Krock, B., Parada-Pozo, G., De la Iglesia, R., Vásquez, M., 2017b. Identification of *Azadinium poporum* (Dinophyceae) in the Southeast Pacific: morphology, molecular phylogeny, and azaspiracid profile characterization. J. Plankton Res. 39 (2), 350–367.

Toebe, K., Joshi, A.R., Messtorff, P., Tillmann, U., Cembella, A., John, U., 2013. Molecular discrimination of taxa within the dinoflagellate genus *Azadinium*, the source of azaspiracid toxins. J. Plankton Res. 35 (1), 225–230.

Trainer, V.L., Moore, L., Bill, B.D., Adams, N.G., Harrington, N., Borchert, J., da Silva, D. A., Eberhart, B.T., 2013. Diarrhetic shellfish toxins and other lipophilic toxins of human health concern in Washington State. Mar. Drugs 11 (6), 1815–1835.

Twiner, M.J., Hess, P., Dechraoui, M.Y., McMahon, T., Samons, M.S., Satake, M., Yasumoto, T., Ramsdell, J.S., Doucette, G.J., 2005. Cytotoxic and cytoskeletal effects of azaspiracid-1 on mammalian cell lines. Toxicon 45 (7), 891–900.

Twiner, M.J., Ryan, J.C., Morey, J.S., Smith, K.J., Hammad, S.M., Van Dolah, F.M., Hess, P., McMahon, T., Satake, M., Yasumoto, T., Doucette, G.J., 2008. Transcriptional profiling and inhibition of cholesterol biosynthesis in human T lymphocyte cells by the marine toxin azaspiracid. Genomics 91 (3), 289–300.

Ueoka, R., Ito, A., Izumikawa, M., Maeda, S., Takagi, M., Shin-Ya, K., Yoshida, M., van Soest, R.W.M., Matsunaga, S., 2009. Isolation of azaspiracid-2 from a marine sponge *Echinoclathria* sp. as a potent cytotoxin. Toxicon 53 (6), 680–684.

Vale, P., Botelho, M.J., Rodrigues, S.M., Gomes, S.S., Sampayo, M.A.d.M., 2008. Two decades of marine biotoxin monitoring in bivalves from Portugal (1986–2006): a review of exposure assessment. Harmful Algae 7 (1), 11–25.

Vilariño, N., Nicolaou, K., Frederick, M.O., Cagide, E., Ares, I.R., Louzao, M.C., Vieytes, M.R., Botana, L.M., 2006. Cell growth inhibition and actin cytoskeleton disorganization induced by azaspiracid-1 structure- activity studies. Chem. Res. Toxicol. 19 (11), 1459–1466.

Vilariño, N., Nicolaou, K.C., Frederick, M.O., Cagide, E., Alfonso, C., Alonso, E., Vieytes, M.R., Botana, L.M., 2008. Azaspiracid substituent at C1 is relevant to in vitro toxicity. Chem. Res. Toxicol. 21 (9), 1823–1831.

Wolf, M., Achtziger, M., Schultz, J., Dandekar, T., Müller, T., 2005. Homology modeling revealed more than 20,000 rRNA internal transcribed spacer 2 (ITS2) secondary structures. RNA 11 (11), 1616–1623.

Wolf, M., Chen, S., Song, J., Ankenbrand, M., Muller, T., 2013. Compensatory base changes in ITS2 secondary structures correlate with the biological species concept despite intragenomic variability in ITS2 sequences-a proof of concept. PLoS One 8 (6), e66726.

Yao, J., Tan, Z., Zhou, D., Guo, M., Xing, L., Yang, S., 2010. Determination of azaspiracid-1 in shellfishes by liquid chromatography with tandem mass spectrometry. Chin. J. Chromatogr. 28 (4), 363–367.